

2

DOT/FAA/CT-88/28

Stall/Spin/Flight Simulation

FAA Technical Center
Atlantic City International Airport
N.J. 08405

AD-A215 719

IC
CTE
18 1989
D

M. G. Nagati
Institute for Aviation Research
Wichita State University

September 1989

Final Report

This document is available to the U.S. public
through the National Technical Information
Service, Springfield, Virginia 22161.

DISTRIBUTION STATEMENT A

Approved for public release;
Distribution Unlimited



U.S. Department of Transportation
Federal Aviation Administration

89 12 18 068

NOTICE

This document is disseminated under the sponsorship of the U. S. Department of Transportation in the interest of information exchange. The United States Government assumes no liability for the contents or use thereof.

The United States Government does not endorse products or manufacturers. Trade or manufacturers' names appear herein solely because they are considered essential to the objective of this report.

1. Report No. DOT/FAA/CT-88/28	2. Government Accession No.	3. Recipient's Catalog No. September 1989	
4. Title and Subtitle STALL/SPIN/FLIGHT SIMULATION		5. Report Date	
		6. Performing Organization Code	
7. Author(s) M. G. Nagati		8. Performing Organization Report No. DOT/FAA/CT-88/28	
9. Performing Organization Name and Address Institute for Aviation Research Whichita State University Whichita, KS 67208		10. Work Unit No. (TRAIS) DTFA03-86-C-00041	
		11. Contract or Grant No.	
12. Sponsoring Agency Name and Address U.S. Department of Transportation Federal Aviation Administration Technical Center Atlantic City International Airport, NJ 08405		13. Type of Report and Period Covered Final Report	
		14. Sponsoring Agency Code ACD-220	
15. Supplementary Notes COTR: John Reed, FAA Technical Center			
16. Abstract This report summarizes the work performed for stall/spin resistant design aids for aircraft. Two major areas were investigated. First, the solution of the non-linear equations of motion with on-line computation of the aerodynamic moments and visual display of the pilot's view and views of the aircraft. This enables evaluation of the simulator and the quality of the solution by pilots and engineers. Second, a method for predicting the aerodynamics of wings near and beyond stall was developed. It serves the purpose of selecting planforms for spin resistant aircraft. This work demonstrates the viability and promise of these approaches against spin.			
17. Key Words Stall, Spin, Configuration Design, Research Simulators Aerodynamics		18. Distribution Statement Document is available to the public through the National Technical Information Service, Springfield, Virginia 22161	
19. Security Classif. (of this report) Unclassified	20. Security Classif. (of this page) Unclassified	21. No. of Pages 65	22. Price

TABLE OF CONTENTS

Introduction	1
The Simulation	1
Computational Evaluation of Wing Planforms	3
Future Work	3
Conclusions	4
Recommendations	4
Appendix A: On Estimating Aircraft Nonlinear Rotary Derivatives From Static Wind Tunnel Data	A-1
Appendix B: Prediction of Planform Modification Effects at High Angles of Attack	B-1
Appendix C: Stall/Spin Flight Simulation, Phase II: Spin Resistant Design and Spin Entry Detection	C-1

Accession For	
NTIS GRA&I	<input checked="" type="checkbox"/>
DDC TAB	<input type="checkbox"/>
USAF	<input type="checkbox"/>
JPL	<input type="checkbox"/>
Pr	
D	
A-1	

1 INTRODUCTION.

1.1 THE SPIN PROBLEM.

The stall departure of general aviation aircraft is a major contributor to aircraft accidents. The desire for designing new aircraft to be spin resistant has been revived in recent years, in order to reduce the chance of inadvertent spin entry is greatly reduced. Another goal is to provide pilot warning when the conditions are favorable for spin entry, and provide it early enough to enable him to take corrective action before aircraft control or excessive altitude are lost.

The work described herein deals primarily with the first goal with two different but related efforts.

1. Development of a real-time visual simulator with interactive controls to enable evaluation of the computer code used, as well as to evaluate aircraft configurations being designed.
2. Development of an aerodynamic prediction method for wing planforms to enable the evaluation of the stall/spin behavior computationally.

1.2 CRITERIA FOR THE DEVELOPMENT WORK.

The techniques developed are simple enough that advanced concept teams with limited computing facilities and budgets can take advantage of them. This means that the visual simulation should be performed on a standard high performance graphics workstation, either stand-alone or in conjunction with a host computer. Near real-time simulation was also necessary so that pilot inputs are easy to apply.

For the aerodynamic prediction code, the method should be based on a well-known technique of solving air flow problems and requiring modest computing resources. Again, this is keeping the configuration design teams in mind.

2. THE SIMULATION.

2.1 EQUATIONS OF MOTION.

In the stall/spin entry regime, the full non-linear coupled equations of motion must be solved as a marching problem. The aerodynamic forces and moments are functions of the motion variables, namely angles of attack and sideslip, velocity and angular velocity. For this reason, the aerodynamic lift and drag are integrated at each timestep over the wing span.

Details of these computations are in Appendix A, a reproduction of a Master's Thesis by J. Ritter on the subject.

2.2 VISUAL SIMULATION.

The results of the numerical solution of the equations of motion at each time step are the three spatial coordinates and the three orientation angles of the aircraft.

These six numbers are used to perform the necessary geometric transformation for the scene to be displayed on the workstation screen. Three options are available and discussed below.

2.2.1 View From the Cockpit.

A scene of the surrounding environment was developed to give the operator a feeling for the rotations and altitude at the current time. The environment consists of a flat terrain with a river and valley. Also included is a sea, two ranges of mountains, a sky and some scattered clouds. This is a simple enough scene to expedite the processing, yet give a good feel for the aircraft motion.

An instrument panel comprised of speed, altitude and rate of climb indicators, an artificial horizon and a compass were added. Also included was a grid to indicate the position of the three controls: rudder, elevator and aileron.

It was learned that including the instrument panel display required an excessive amount of processing time, thus making it impossible to achieve real-time simulation. It was therefore removed temporarily, until code optimization can be performed.

2.2.2 View From The Ground.

A view of the environment scene plus the aircraft from a fixed point on the ground (zero altitude) can be achieved in this option. A hidden surface algorithm was developed to display the aircraft realistically. The method is to generate an aircraft-fixed coordinate system, and at each time step, determine which octant of the coordinate system the view point occurs. One of eight possible sequences for drawing the panels of the aircraft is then performed, depending on which octant is selected. A zoom feature is also employed.

2.2.3 View From A Flying Observer.

Because of limits on the zoom angle in the above option, the aircraft appears very small when at high altitudes. A moving viewpoint was provided as a third option to simulate the view from an observation aircraft flying parallel to the object aircraft, except it does not spin or rotate. This viewpoint is displaced from the object aircraft by a fixed vectorial length. In addition to being closer, thus viewing the aircraft better, the effect of change in the line of sight, which could be misleading, is eliminated. This also simulates the observers view in a spin tunnel test. All the other features of Section 2.2.2 are included here.

2.3 HARDWARE.

Even though it was originally intended to perform the solution of the equations of motion on a host computer, limitations on the data transfer rates of the Ethernet made it difficult to modify the program structure to take advantage of certain features of the workstation. Alternatives include Direct Memory Access (DMA) devices, which limit the physical distance between the host and the terminal.

The ideal solution may be to use a super workstation with higher computation speed and to obtain advanced training for taking full advantage of the system capabilities. A full-scale Learjet cockpit simulator was acquired from Learjet Company recently. This will be fitted with visual display and will employ the cockpit controls in future work.

3. COMPUTATIONAL EVALUATION OF WING PLANFORMS.

Most computer codes available today are either limited to low angle of attack, small perturbation aerodynamic analysis, or require considerable modeling and computing power. An example of the latter is the Navier-Stokes codes which run on super computers and are difficult to use. These codes have not yet reached the level of reliability which would permit preliminary designers to use them.

This part of the current effort provides a method which uses the familiar, efficient, and reliable panel codes with minor modifications. This technique and its application to a wing are detailed in Appendix B.

4. FUTURE WORK.

Building on the experience of current work, the following objectives are identified to provide industry and government with a research and development facility which deals with pre-prototype and pre-wind tunnel study of the spin entry problems. This will enable configuration designers to evaluate their concepts more thoroughly for a safer or more effective design, and government (regulators and monitors) to better understand the problems associated with this and other unusual aircraft configurations and flight conditions in order to establish specifications, criteria and regulations.

These goals are seen to be as follows:

1. Upgrade computational capability which is intended to support real-time flight simulation with graphics, a cockpit, and associated instrumentation and controls with force feedback. It is also intended to support the computational solutions of aerodynamic loads. This includes the setup overall computing system: interfaces; D/A, A/D converters, servos for stick force, graphics

drives, communication, etc. and the development of more experience with the system by attending seminars, and using software support services to develop more efficient computational schemes.

2. Further development of the Aerodynamic loads prediction techniques to include:
 - a. Very large angles of attack.
 - b. Large angular rates
 - c. Arbitrary wing planforms.
 - d. Control surface effectiveness.
 - e. Fuselage effects (wing wake effect on fuselage).
 - f. Propeller effects.
 - g. Selection, acquisition and implementation of a suitable alternative to the present paneling code for high angular rates.
 - h. Develop methodology for aerodynamic computations on-line with the motion simulation.
 - i. Extension to transport-type aircraft planforms.

* Note that d & e are required to study spin recovery.
3. Development of "Spin Warning" Devices for alerting pilots of conditions which may lead to spin entry, and the development of optimal spin recovery techniques (i.e., with minimum loss of altitude.)

5. CONCLUSIONS.

1. Tools for evaluation of aircraft configurations and their proneness to spin entry have been developed which show significant progress toward more comprehensive evaluation methods.
2. For the visual simulation, more efficient computer codes and/or higher performance devices (now available) are desirable for better results.
3. For the aerodynamic prediction, code improvement and more validation with wind tunnel or other experimental results are required. In addition, rotational rates to simulate aircraft rotation and spin condition should be incorporated.

6. RECOMMENDATIONS.

The recommendations for further work are outlined in the proposal summarized in Appendix C.

APPENDIX A

On Estimating Aircraft Nonlinear Rotary Derivatives From Static Wind Tunnel Data.

James R. Ritter
The Wichita State University

ABSTRACT

One problem in mathematical modeling of aircraft post-stall behavior lies in the difficulty in describing aerodynamic moments due to airplane rates of rotation. In particular, the rolling and yawing rate derivatives $C_{\dot{p}}$, $C_{\dot{r}}$, $C_{n\dot{p}}$ and $C_{n\dot{r}}$ are crucial to accurate motion modeling. These derivatives are not constant values when the linear assumptions of unstalled flight are abandoned. One method for calculating these derivatives was applied to a low-wing, single-engine general aviation airplane for which sufficient, high angle-of-attack wind tunnel data is available. This method involves approximations that limit the validity of the model and produce unsatisfactory results when used in an established spin modeling program and compared with extensive, full-scale flight test results. By using a new method and an extended computational technique, a better match with flight test data was obtained. The response to controls during stall departure is characteristic of the subject airplane when the new derivatives are used. Unlike the old derivatives, the new ones are sensitive to variations of the state space parameters, and in a predictable manner. Sensitivity to aerodynamic spanwise loading is also evaluated. Comparisons are made between the old and new derivatives, and between outputs of otherwise identical executions of the spin program.

Table of Contents

Abstract - - - - -	1
Table of Contents - - - - -	2
A List of Symbols - - - - -	3-6
Some Nomenclature - - - - -	7,8
Introduction - - - - -	9
The Problem - - - - -	9-11
The Wykes Equations - - - - -	12
The Ritter Functions - - - - -	12,13
Discussion Concerning the Wykes and Ritter Methods - - - - -	13-15
A Sample Comparison - - - - -	15-18
The Evaluation - - - - -	19-24
Conclusion - - - - -	25
References - - - - -	26
 Appendix A: Pressure Data on the Wing - - - - -	 27-31
Appendix B: The Ritter Equations - - - - -	32-42
Appendix C: Bihrlé Derivatives and Ritter Functions Compared - - - - -	43-48
Appendix D: Sensitivity to Spanwise Force Distribution - - - - -	49-52

A List of Symbols

b	wing span (feet)
b.f.	blockage factor
C.G. or c.g.	center of gravity
C_l	rolling moment coefficient, $C_l = \frac{M_x}{q_\infty S b}$
$C_{l_{n.r.}}$	rolling moment coefficient, non-rolling airplane
C_L	3-d lift force coefficient
C_{lp}	rolling moment due to rolling motion coefficient, a rate derivative ("damping-in-roll"), $C_{lp} = \frac{\partial C_l}{\partial (p b / 2 V)}$
C_{lr}	rolling moment due to yawing motion coefficient, a rate derivative, $C_{lr} = \frac{\partial C_l}{\partial (r b / 2 V)}$
C_N	3-d normal force coefficient
C_n	yawing moment coefficient, $C_n = \frac{M_z}{q_\infty S b}$
C_{N_1}	section normal force coefficient at station 1
C_{np}	yawing moment due to rolling motion coefficient, a rate derivative, $C_{np} = \frac{\partial C_n}{\partial (p b / 2 V)}$
C_{nr}	yawing moment due to yawing motion coefficient, a rate derivative ("damping-in-yaw"), $C_{nr} = \frac{C_n}{\partial (r b / 2 V)}$
d_i	a distribution factor at station i

Symbols (continued)

F_L	a general force on the left wing; direction is implied from the context
F_R	a general force on the right wing; direction is implied from the context
i	a wing station designator variable
\bar{L}	rolling moment (foot-pounds)
L	lift (pounds), left
l_v	length from airplane c.g. to the vertical tail center of pressure (feet)
m	slope of a curve; the incremental change in the ordinate with respect to the abscissa at a point on the curve
n.d.	non-dimensional
p	roll rate (radians per second)
q_L	local dynamic pressure (pounds/sqr. foot)
q_∞	freestream dynamic pressure (lb./sqr. foot)
r	yaw rate (radians per second)
R	right
R.P.M.	revolutions per minute
S_{e_i}	effective strip area at station i (ft ²)
S_w	Total wing planform area (ft ²)
S_{we}	effective planform area, the sum of all the strip areas, one side only (ft ²)
t	time (seconds)
T.E.	trailing edge (of a wing or control surface)
u	body motion velocity with respect to the atmosphere, direction is parallel to the roll (x-body) axis (ft/sec)
v	body motion velocity with respect to the atmosphere, direction is parallel to the pitch (y-body) axis (ft/sec)
V	velocity (ft/second)

Symbols (continued)

$V_{i_{roll}}$	The product of rotation rate and station span arm to the rotation axis (ft/second)
V_L	velocity at or very near the airplane surface (ft/second)
V_∞	velocity in the freestream (ft/second)
w	body motion velocity with respect to the atmosphere, direction is parallel to the yaw axis (ft/sec)
y_i	distance from the airplane center of mass to a wing station; may be in feet or non-dimensional

Greek Symbols

α	an aerodynamic angle-of-attack, the angle between the longitudinal axis and the flight path tangent in the vertical plane (degrees)
α_i	angle-of-attack at station i (degrees)
α_A	angle-of-attack of the airplane
α_w	angle-of-attack of the wing; differs from angle-of-attack of the airplane by the wing incidence with respect to the airplane longitudinal axis (degrees)
β	an aerodynamic angle-of-attack, the angle between the longitudinal axis and the flight path heading; also called the sideslip angle (degrees)
Δ	change in

Some Nomenclature

alpha	angle-of-attack in the vertical plane (see α)
angle-of-attack	the angle between a body axis and the wind
attractor [*]	an equilibrium state that attracts trajectories; trajectories need not enter an attractor to be affected by it; trajectories need not interact in a clearly defined fashion (chaotic attractor)
beta	side slip angle (see β)
flat spin	a spin in which the airplane attitude is relatively flat with respect to the ground; alpha is generally greater than 1 radian
limit cycle [*]	a closed trajectory; a helix in the case of the path of a spinning or spiraling airplane; other aircraft motions not so easily defined
pitch	aircraft attitude in the vertical plane
rate derivative	a derivative of a moment with respect to a rotary motion
rectangular distribution	a uniform distribution of forces across the wing span
rotary derivative	see rate derivative
Schrenk	a spanwise distribution approximation that averages the planform width distribution with an elliptical one
spin	a high angle-of-attack helical flight path of negligible helix radius
spiral	any helical flight path where the helix radius is large, generally greater than one wing span
stability derivative	a partial derivative of a force or moment with respect to a motion
stall	a sudden separation of flow on the wing that typically results in a flight condition that is unstable in pitch, roll and yaw

Nomenclature (cont.)

state space*	a geometric model for the set of all idealized states of an organism; the state space is filled with trajectories and is called the phase portrait of a dynamical system
steep spin	a nose-low spin in which alpha is moderate, generally less than 1 radian
trajectory	the time rate-of-change of a state variable

* These terms are part of the language of the geometry of behavior, discussed by Abraham and Shaw⁽¹⁾

On Estimating Aircraft Nonlinear Rotary
Derivatives From Static Wind Tunnel Data

James R. Ritter
The Wichita State University

Introduction

Most flight regimes permit linear modeling of the aerodynamic forces and moments as functions of the motion variables. This allows the definition and use of what are called stability derivatives, which are the partial derivatives of forces or moments, either in dimensional or non-dimensional form, with respect to motion variables such as velocity, angle of attack, rotational rates and so forth. Such derivatives are taken to be constants for a given flight regime in the linear model.

In the approach to stall, and particularly in the post-stall maneuver, significant angular rotation rates develop. These rates cause linear approximations to be invalid, primarily because of the aerodynamic forces on the wing resulting from roll and yaw rates. In stall/spin maneuvers, the partial derivative constants of stability must be replaced by forces and moments which are functions of more than one argument of the motion variables.

The Problem

Aerodynamic forces and moments can be defined quantitatively in the wind tunnel, but once the airplane begins to rotate in post-stall departure, static-flow measurements are not directly representative. There are numerous schemes for evaluating ro-

tating forces and moments, either by rotating or shearing the airflow, or by rotating the model in a static flow field, and all add a great deal of complexity to the management and collection of data. There has been some hope that rotational aerodynamics can be derived from static wind tunnel data. Methods used heretofore are attempts to retain some of the simplicity afforded by stability derivatives, but make them functions of a single argument rather than constants. Since the wing is the major contributor to motion during the stall/spin, efforts will focus on an improved method for the four rate derivatives governed by the wing aerodynamics, C_{l_p} , C_{n_p} , C_{l_r} and C_{n_r} .

Consider the local angle of attack across the span of a wing when significant roll and yaw rates are present in the airplane motion (Figures 1,2, and 3):

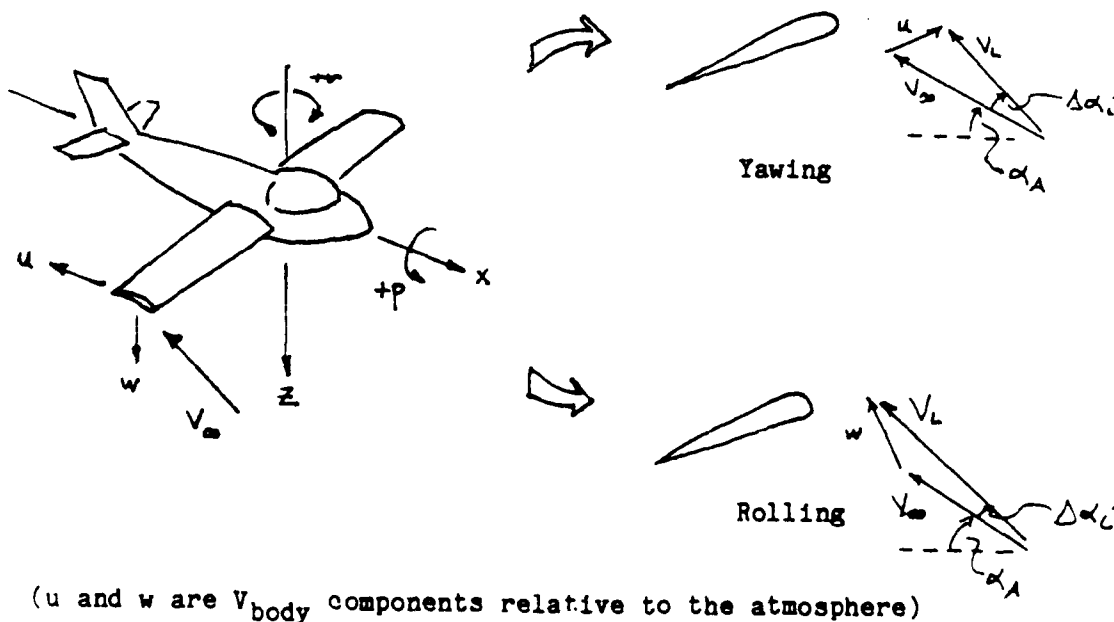


Figure 1: Local V and α , Rolling And Yawing

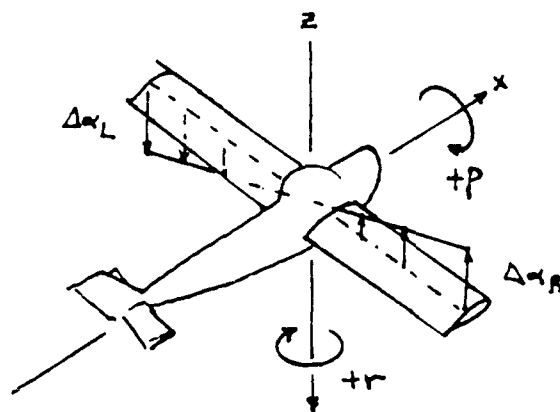


Figure 2: Local Angle of Attack Alpha
Dominant Rolling Shown

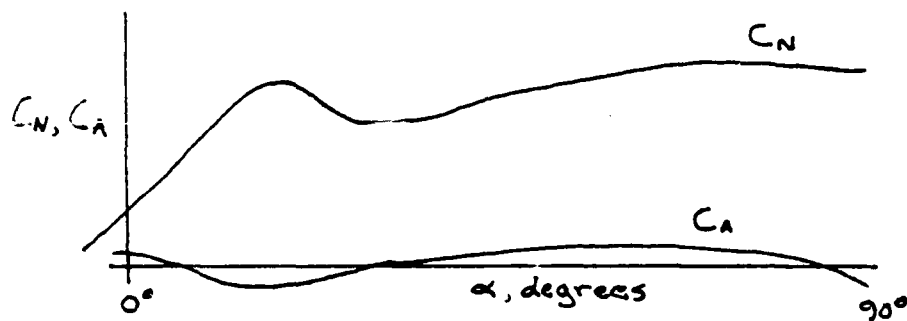


Figure 3: C_N, C_A vs. α

This means:

- a.) local normal and axial forces vary across the span,
- b.) a spanwise distribution must be assumed, typically as per Schrenk or rectangular, and
- c.) local dynamic pressure varies across the span due to velocity increments due to roll and yaw.

Thus roll and yaw moments become functions of four arguments which must be determined by integrating across the span of the wing, i.e., $C_l = C_l(\alpha, V, p, r)$ and $C_n = C_n(\alpha, V, p, r)$

(see Appendix B).

The Wykes Equations

One formulation used for converting static aerodynamics to rotating aerodynamics has already been made⁽²⁾, and the ensuing derivations are hereafter referred to as the Wykes equations.

The Wykes derivations are the result of a quasi-static, wing-panel strip integration scheme that determines rate derivatives as single-variable functions of airplane angle of attack α . This method of derivation is accomplished by using a simple, closed-form approach to the solution, and as a result the Wykes equations are independent of aircraft motion to a large degree.

The researcher who first used the Wykes equations to investigate the rate derivatives of a low-wing, single-engine general aviation trainer presented his results in a report⁽³⁾ composed chiefly of plots (hereafter called Bihle derivatives), very basic descriptions of methods, and a list of the Wykes equations. A clue to more specific procedures comes from an earlier report⁽⁴⁾ in which the Wykes equations were used to determine the rate derivatives of a Navy trainer. In that report, sample derivations are included, reflecting for example the use of an elliptical lift distribution and a strip integration resolution of five strips per side.

The Ritter Functions

As a simple and expedient means of distinguishing between methods to obtain derivatives, the rotational aerodynamic moments developed in this thesis will hereafter be called Ritter

functions. The Ritter functions vary in accordance with the premise that the difference between wing panel moments is dependent on the rates themselves and on the velocity of the airplane in a specific way. The Ritter functions depend on the chosen state variables of the system in a non-differentiable way; consequently, these functions are not themselves derivatives. They define moment coefficients, replacing those that are normally defined in the spin equations by multiplying the rates with the rate derivatives. The Ritter technique requires only static wind tunnel data, not rotary balance data or data from other methods, and these static data are available for the subject airplane⁽⁵⁾.

Discussion Concerning the Wykes and Ritter Methods

Stall departure and spins involve significant angular rotation rates, and the primary influence of rotational motion, particularly in roll and yaw, comes from the variation in local angle of attack across the span of the wing. The variable C_{l_p} , which in coefficient form represents rolling moment (l) caused by rolling motion (p) about the longitudinal axis, is chosen to compare the methods of Wykes and Ritter.

In the development of C_{l_p} , aerodynamic forces across the span of, and normal to, the planform of the wing are considered to act perpendicular to their respective span distances from the rolling axis to produce a net rolling moment. The continuous nature of the force distribution is approximated by partitioning the span of the wing into strips and either assuming a spanwise force distribution such as elliptical or rectangular or

Schrenkian, or by using measured pressure data⁽⁶⁾ from which force data can be derived (Appendix A). When the moments are integrated by summation over left and right wing semi-spans, a net differential moment is the result. The calculation is repeated over and over for a full range of airplane alphas (angles-of-attack) which the aircraft is expected to encounter during stall departure and spin.

In the derivation of the equations of motion⁽⁷⁾, the rate derivatives were assumed to be single variable functions of angle of attack alpha, as per Wykes. The moment coefficients C_l and C_n were reconstituted from these assumed derivatives and their respective angular rates during motion integration:

$$C_l = C_{l_{n.r.}} + C_{l_p}(\alpha) \times p + C_{l_r}(\alpha) \times r \text{ and}$$

$$C_n = C_{n_{n.r.}} + C_{n_p}(\alpha) \times p + C_{n_r}(\alpha) \times r$$

For the Ritter method, the moments are calculated more directly. In essence, local angle of attack at each i^{th} wing station is found from V , p , and r ; local dynamic pressure is calculated for each station; local section normal and axial force coefficients are found at each station; force and subsequently moments are found at the i^{th} station and then summed over both wing panels. The equations are:

$$C_l = C_l(\alpha, V, p, r) = - \sum_R C_{n_i} y_i \left(\frac{V_i}{V_\infty} \right)^2 d_i \frac{S_{w_i}}{S_{w_c}} + \sum_L C_{a_i} y_i \left(\frac{V_i}{V_\infty} \right)^2 d_i \frac{S_{w_i}}{S_{w_c}}$$

$$\text{and } C_n = C_n(\alpha, V, p, r) = \sum_R C_{a_i} y_i \left(\frac{V_i}{V_\infty} \right)^2 d_i \frac{S_{w_i}}{S_{w_c}} - \sum_L C_{n_i} y_i \left(\frac{V_i}{V_\infty} \right)^2 d_i \frac{S_{w_i}}{S_{w_c}}$$

where R and L refer to right and left wing panels.

$C_{N_1} = C_{N_1}(\alpha_A, \Delta\alpha_1)$ is the normal force coefficient at wing station 1,

$\frac{V_1}{V_\infty} = \frac{V_1}{V_\infty}(p, r)$ is the local-to-freestream velocity ratio, representative of the dynamic pressure ratio,

y_1 is the moment arm from station 1 to the roll axis of the airplane,

d_1 is a distribution factor at station 1 (Schrenk, elliptical, rectangular, experimental, etc.),

S_{e_1} is the effective load area for wing panel strip representation, and

S_{w_e} is the total planform wing area S_w minus the area blocked by the fuselage, and minus other areas not represented in the strip integration scheme.

Details of the derivations may be found in Appendix B.

This kind of multi-variable representation means that highly repetitive and often redundant calculations are required for determining stability moments -- the elegant but less-than-accurate method of Wykes must be replaced with an extended computer technique.

A Sample Comparison

The difference between Wykes and Ritter can be described in the context of the following figure (Figure 4).

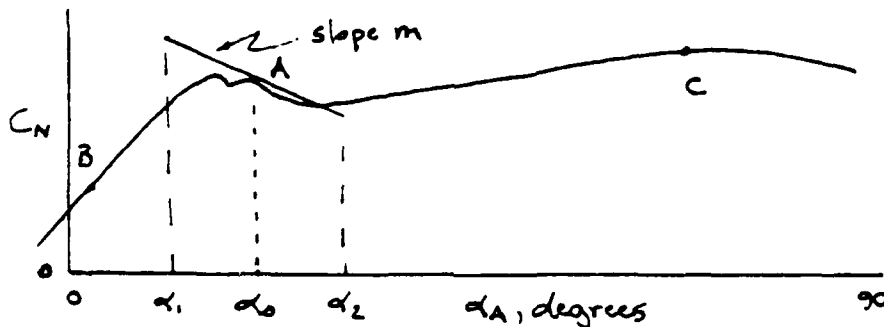


Figure 4: C_N vs. α , Local α Variation

The above figure is a plot of the wing normal force coefficient C_N as it varies with airplane angle-of-attack α . Point

A occurs at example α_c . In the Wykes method, the slope m at A is used to project the C_N condition at each wing partition location. This method is satisfactory at points B or C where the slope is more or less constant, or anywhere the roll rate and thus the α variation is very small. But in the region around point A, the slope is not constant. The airflow becomes increasingly unsteady on both wing panels, left and right; intuitively, the resultant normal forces on each panel may be quite different at any given instant, resulting in a large moment one way or the other, and subsequently a high roll acceleration. A roll rate of 150 degrees per second (Figure 8) for an airplane traveling at a speed of 120 feet per second (Figure 6) means wing tip speeds of $(\pi/180) \times (150) \times (12.25) = 32.1$ feet per second ($V_{roll} = \omega \times r$) and an increased (or decreased) angle of attack of approximately 15 degrees:

$$\Delta\alpha \cong \arctan (V_{roll}/V_{\infty}) = \arctan (32.1 / 120) = 15 \text{ degr.}$$

The Wykes derivative thus fails to be consistently representative since the difference between wing tip alphas can be as great as 30 degrees. Dynamic pressure also varies in a way that compounds the problem for positive alpha, positive roll rate (Appendix B).

Wykes' method is concluded by taking the derivative of roll moment with respect to roll rate and plotting the results. In contrast, the Ritter method is ideally concluded at the derivation of the net moment. There is no way to plot Ritter functions that is consistent with the premise that each moment coefficient be evaluated at each instant in time with respect to all relevant state variables, but the Ritter functions can be evaluated and

compared with the Bihrlé derivatives if a set of fixed conditions is chosen. A baseline of variables is selected, in which velocity is 120 feet per second and roll rate is one radian per second. A pseudo-derivative curve (C_l/p , C_n/r , etc.) is then produced that is representative of the selected states. The curves of Ritter and Bihrlé "derivatives" are plotted and compared in Figure 5.

The same method used to calculate the C_l/p function is used to calculate C_l/r , C_n/p , and C_n/r functions. The four derivatives of the Wykes method are shown in Appendix C and compared with the specific parametric evaluations of the Ritter functions as in Figure 5. (The Wykes and Ritter methods might be expected to compare favorably when the roll rate is small; a roll rate of .1 rad/second is evaluated and the comparison is as expected.)

One unknown condition that required investigation was spanwise distribution. Integrated pressure distributions⁽⁸⁾ and two assumed distributions, rectangular and Schrenk, are compared in Appendix D. There are some small differences in two of the derivatives when pressure data is compared with the assumed methods. These differences are attributed to inconsistencies between force and pressure data, and to the varying flow in the alpha range investigated (11.2 to 41.5 degrees). There is no noticeable difference between rectangular and Schrenk distributions when considering a baseline set of state variables ($V = 120$ ft/sec and p and $r = 1$ rad/second).

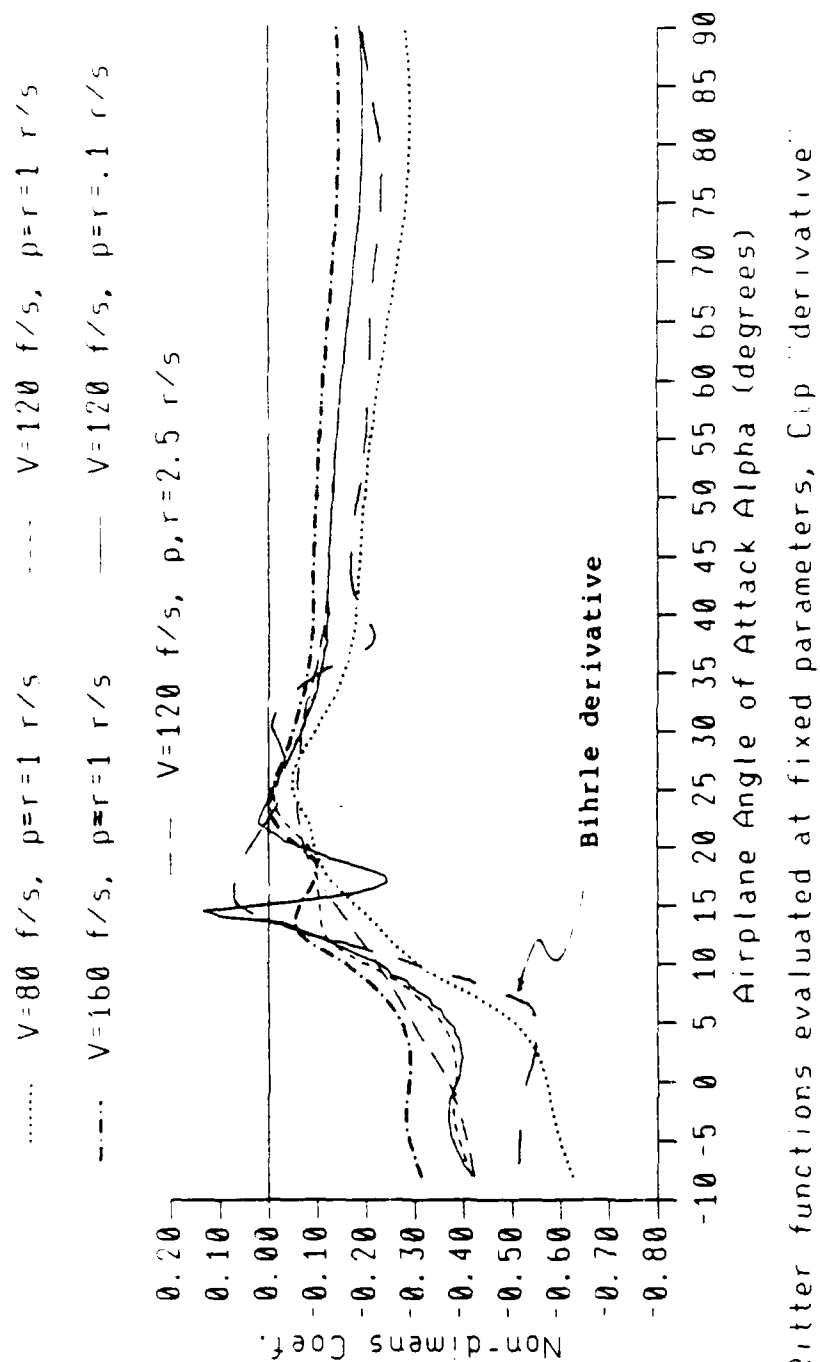


Figure 5: Bihrlé C_{lp} vs. the Ritter Function $C_l(\alpha, V, p)$
 Evaluated at Different Sets of Fixed Parameters

The Evaluation

The complex behavior of an aircraft in stall or in spin can be described symbolically as the solution of a set of first-order differential equations in which both the kinematic and aerodynamic terms involve nonlinearities. In solution, no limit cycle can be readily described; nevertheless, actual spin behavior is mode-like, and the attractor or attractors (many airplanes have more than one) can be most easily evaluated through numerical integration and plotting.

A great many full scale flight test time histories exist for the subject aircraft from NASA spin research⁽⁹⁾. This means an actual result is available to prove or disprove a model. A six-degree-of-freedom model of the equations of motion⁽¹⁰⁾ has been used for five years at Wichita State University in spin research⁽¹¹⁾. These equations are without restriction in the limits of motion, and contain fully nonlinear kinematic terms. The Ritter functions provide a complementary set of compatible, nonlinear aerodynamic terms.

A program was written to evaluate the Ritter method. It was used independently to generate the specific, single-variable derivatives in Figure 5 and in Appendices C and D. An evaluation of spin behavior that is consistent with the premises concerning the state-dependent nature of the derivatives as functions is made by incorporating this program into the spin program as a subroutine, thus replacing piecewise linear fits of the Bihrlé derivatives. The spin solutions using the Bihrlé derivatives and the Ritter functions are then compared with each other and with

flight test data (Figures 6, 7, 8, and 9).

A flight test spin was chosen which reflects a varied, full-range application of elevator and rudder. These control profiles have been modeled in the spin program and plots of three key trajectories, α , p , and r , are compared on the following pages.

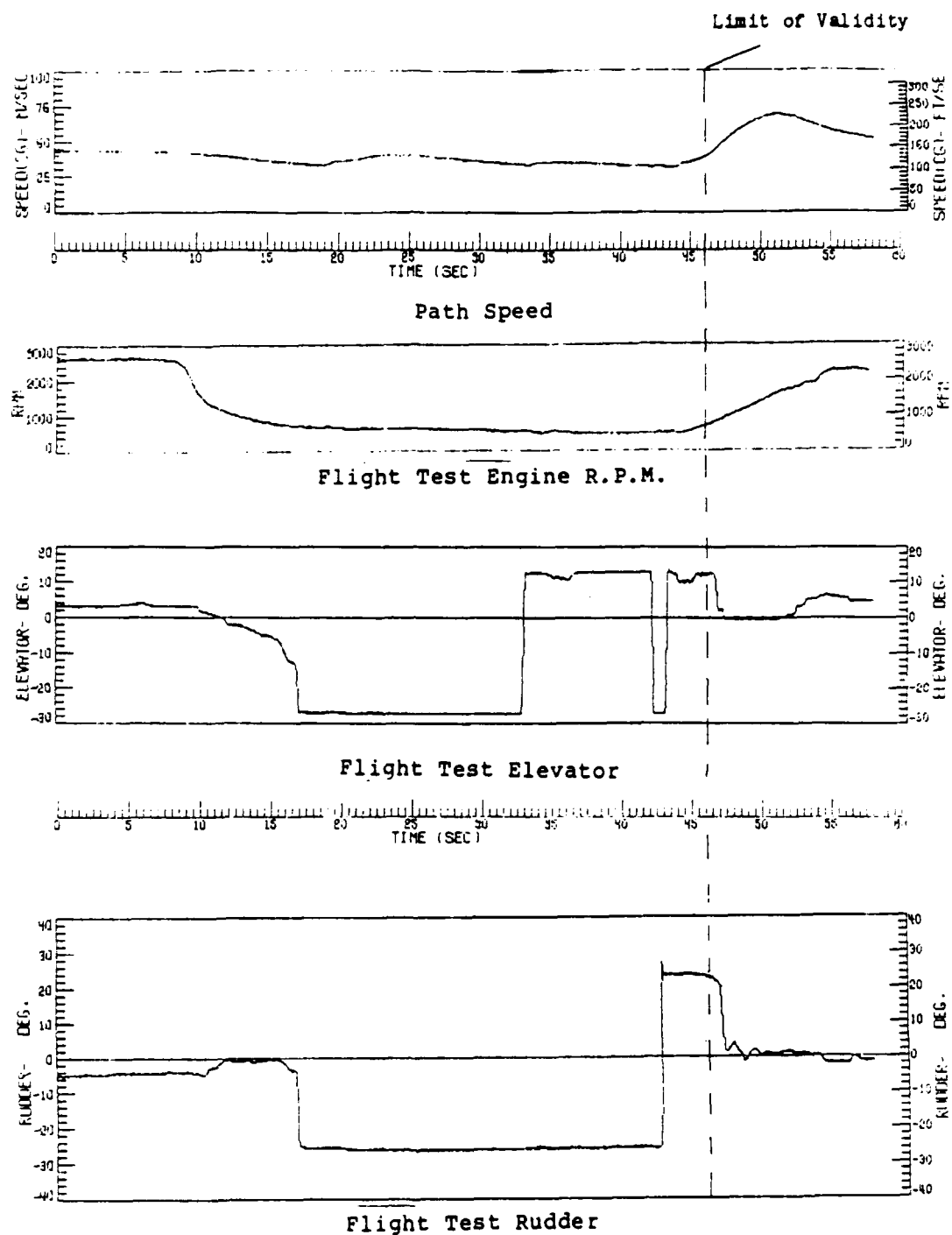


Figure 6: Flight Test of a Low-Wing, Single-Engine General Aviation Airplane in Spin: Speed, Power, Elevator and Rudder Profiles

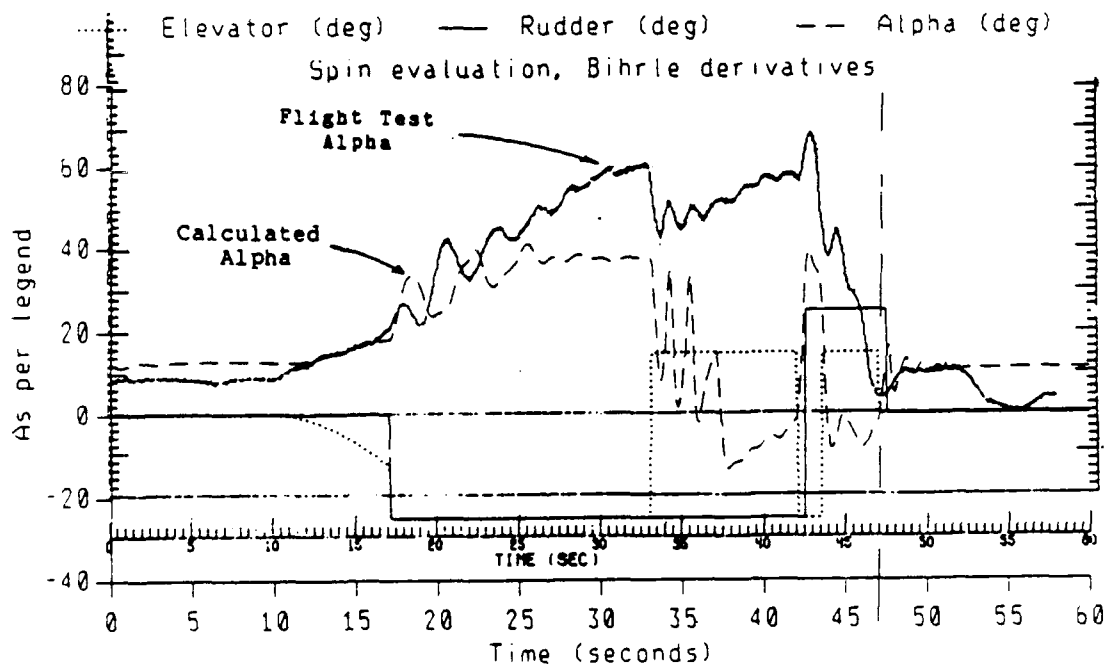
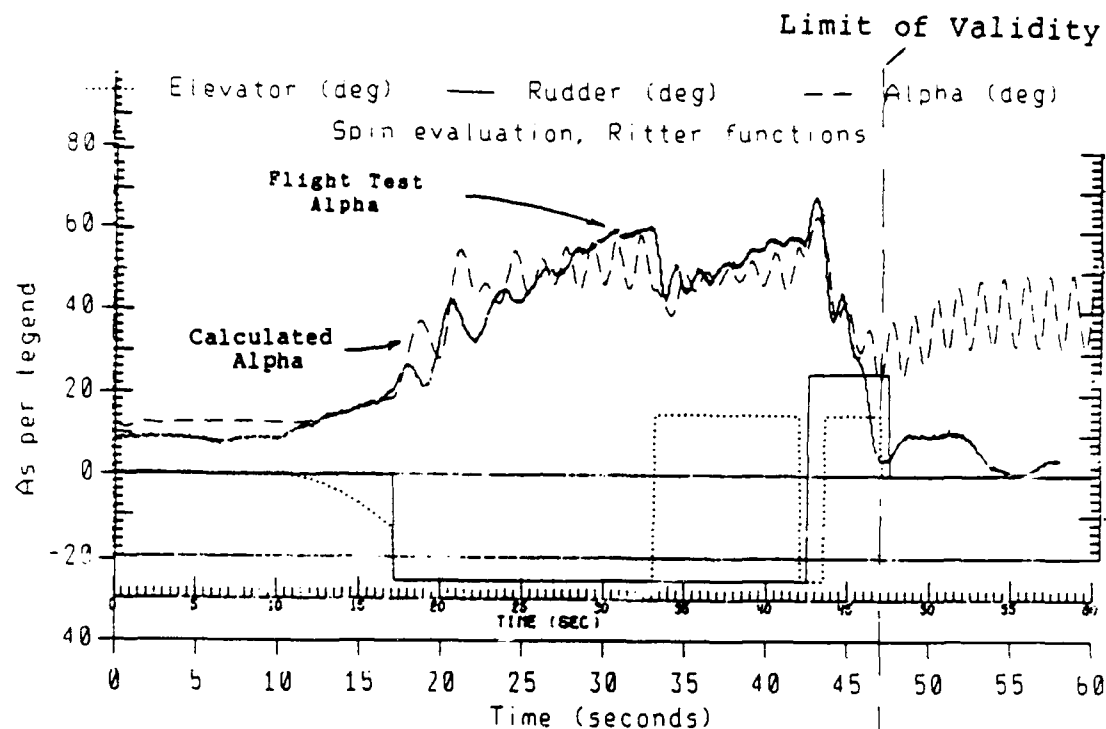


Figure 7: Flight Test vs. Bihrlé and Ritter Spins:
Airplane Angle-of-Attack Alpha

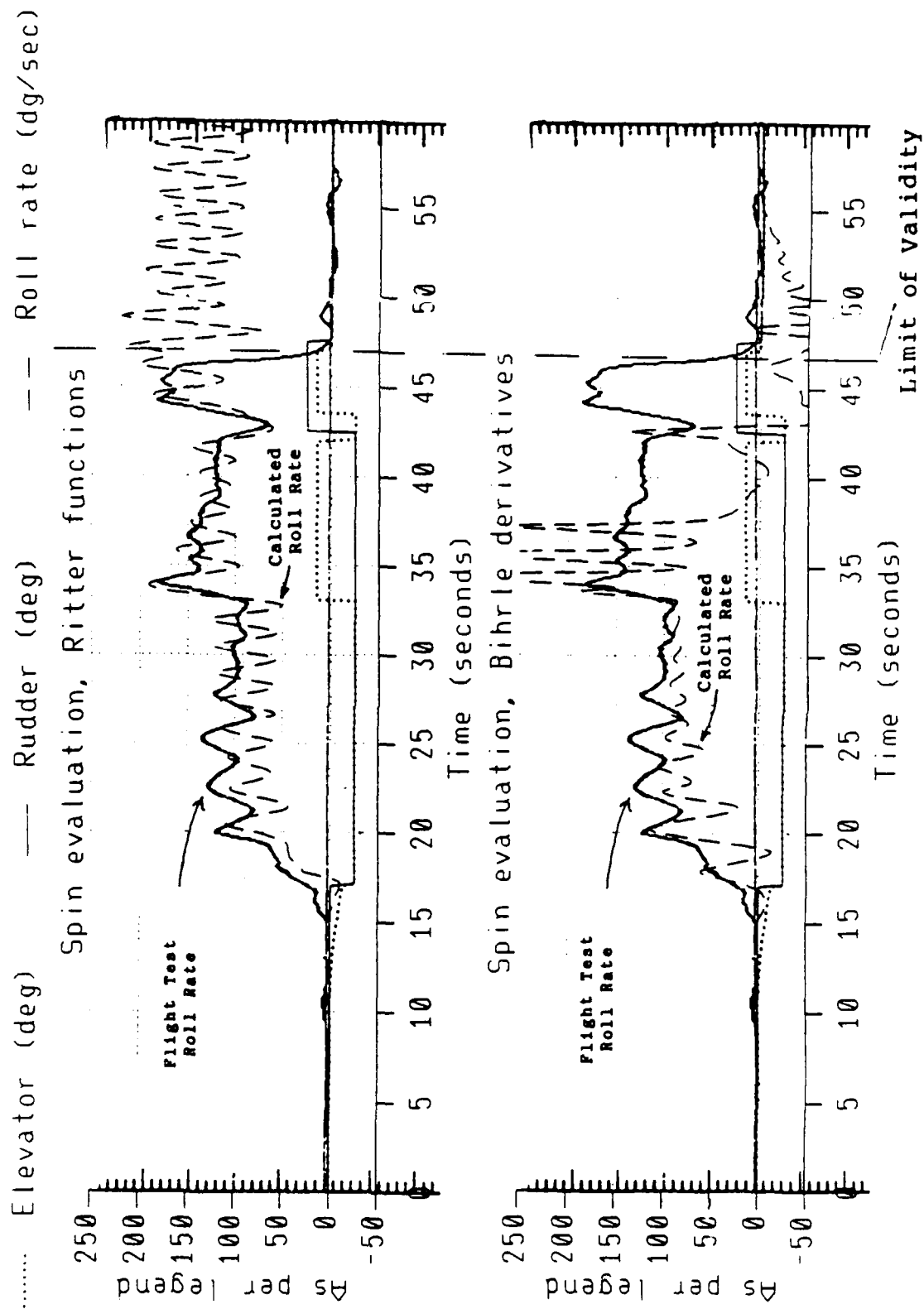


Figure 8: Flight Test vs. Bihrlé and Ritter Spins:
Roll Rate

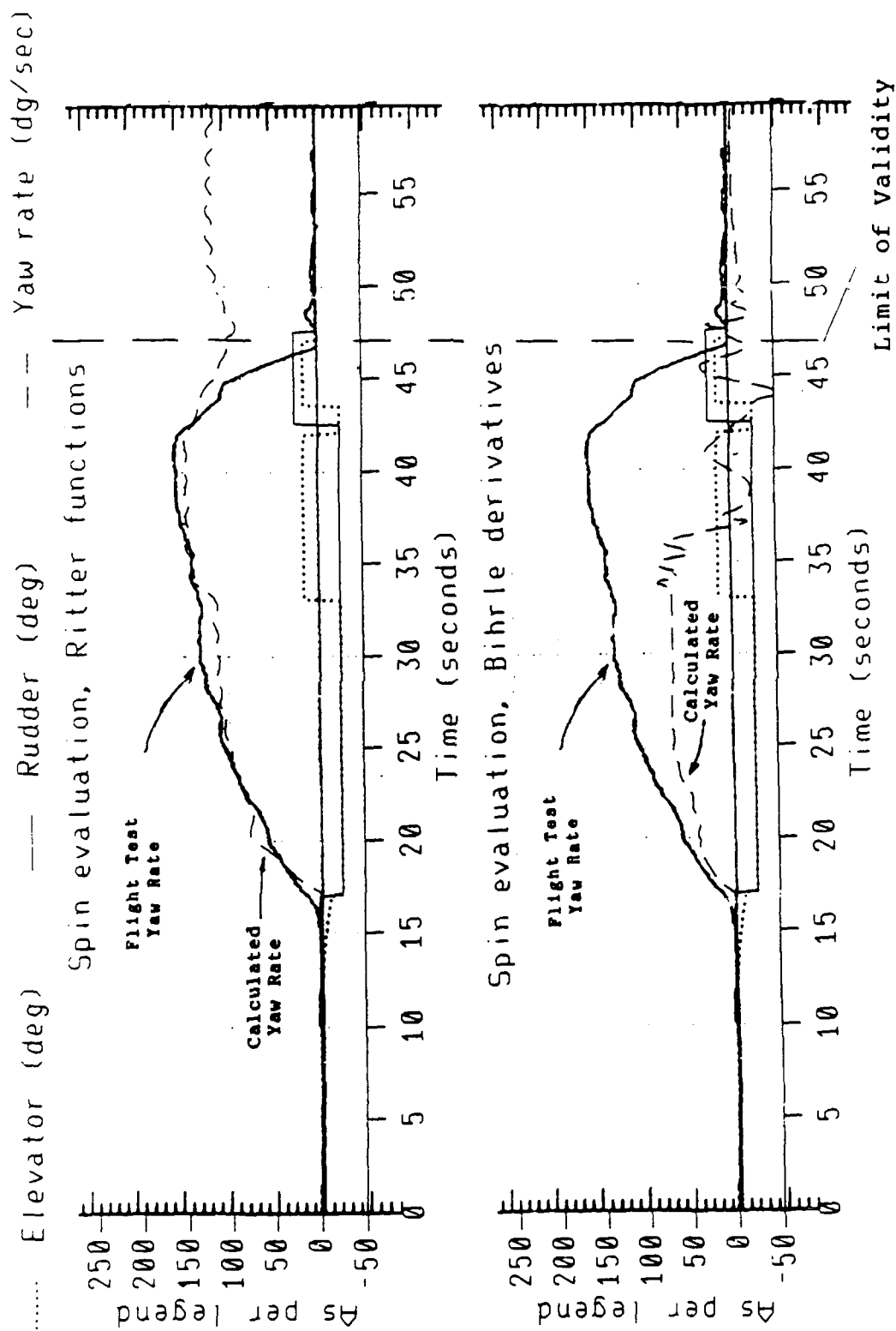


Figure 9: Flight Test vs. Bihrlé and Ritter Spins:
Yaw Rate

Conclusion

The Bihrlé derivatives, based on the Wykes equations, were used in a flight simulator program as a means of qualifying spin behavior. The response to controls had been shown to be very sensitive in early studies; nevertheless, the variable derivatives were effective in producing a spin. The Ritter functions have produced a more realistic departure and response to controls up until the point where power was added during flight test recovery. Engine thrust has not been modeled in the spin program; hence, a Limit of Validity has been established in Figures 6 through 9 defining that point in time.

The improved behavior using Ritter functions is ascribed at least in part to the expanded concept used in defining the rate derivatives, that the moments C_n and C_l are functions of α , p , r , and V and can be defined numerically and in a consistent manner from within the research spin program.

References

1. Abraham, Ralph H., and Shaw, Christopher D., Dynamics -- The Geometry of Behavior, Aerial Press, Santa Cruz, Ca, 1985
2. Wykes, John H., Casteel, Gilbert R., and Collins, Richard A., An Analytical Study of the Dynamics of Spinning Aircraft. Part 1. Flight Test Data Analysis and Spin Calculations, WADC TR 58-381, Part I, 1958.
3. Bihrlle, Jr., William, Estimated Dynamic Aerodynamic Derivatives for the LWGA (Yankee) for the -8 to 90 Degrees Angle of Attack Range, Bihrlle Applied Research, Inc., BAR 79-1M, 1979.
4. Barnhart, Billy, Estimated Dynamic Derivatives for T-2C Aircraft From -8 to +45 Degrees Angle of Attack, NASA Report NADC-75367-30, 1976
5. Bihrlle, Jr., William, Barnhart, Billy, and Pantason, Paul, Static Aerodynamic Characteristics of a Typical Single-Engine Low-Wing General Aviation Design for an Angle-of-Attack Range of -8 to 90, NASA Contractor Report 2971, 1979
6. Newsom, Jr., William A., Satran, Dale R., and Johnson, Jr., Joseph L., Effects of Wing-Leading-Edge Modifications on a Full-Scale Low-Wing General Aviation Airplane: Wind-Tunnel Investigation of High-Angle-of-Attack Aerodynamic Characteristics, NASA Technical Paper 2011, 1982
7. Adams, Jr., William M., Analytic Prediction of Airplane Equilibrium Spin Characteristics, NASA Technical Note D-6926, 1972
8. Newsom, idem
9. Stough, III, H. Paul, L.G.A.S. Spin Project, Flt 45, run 3SP31, NASA-Langley, 1979
10. Adams, Jr., idem
11. Staples, David L., A Computer Model of Light-Plane Spin Departure. Master's Thesis, The Wichita State University, 1984.
12. Newsom, idem
13. Bihrlle, Jr., Static Aerodynamic Characteristics...idem
14. Bihrlle, Jr., Established Dynamic Aerodynamic...idem

Appendix A: Pressure Data and Wind Tunnel Force Data

Researchers at NASA collected wing pressure data for the full-scale test airplane airplane angles-of-attack 11.2, 21.6, 31.9, and 41.5 degrees⁽¹²⁾. A pressure integration program was written to evaluate the normal and axial forces at the six spanwise locations selected for pressure testing.

The pressure tests are substantive along the chord and are used to evaluate absolute pressure forces in the region of each spanwise station. A unit width of one inch is considered at a point of measurement, surface length segment boundaries are shared between pressure ports, and the product of width segment and length segment is the local area at each port.

A B-spline curve fit is used on the upper and lower surfaces to evaluate the slope at all points respective to the chord reference line. The pressure forces are first evaluated perpendicular to the surface. The components of each force normal to the longitudinal axis of the airplane are collected along the section line and summed to yield a normal pressure force on the wing at that wing station. Similarly, axial components are collected and summed. The result is a set of six normal and six axial forces across each wing panel, left and right sides. The profile of the forces in each direction is a representation of the force distribution.

In order that these distributions be in some way compatible with distributions, Schrenk or otherwise, that must be assumed outside the pressure tested alpha range, the pressure distributions are normalized to a value of one. The general

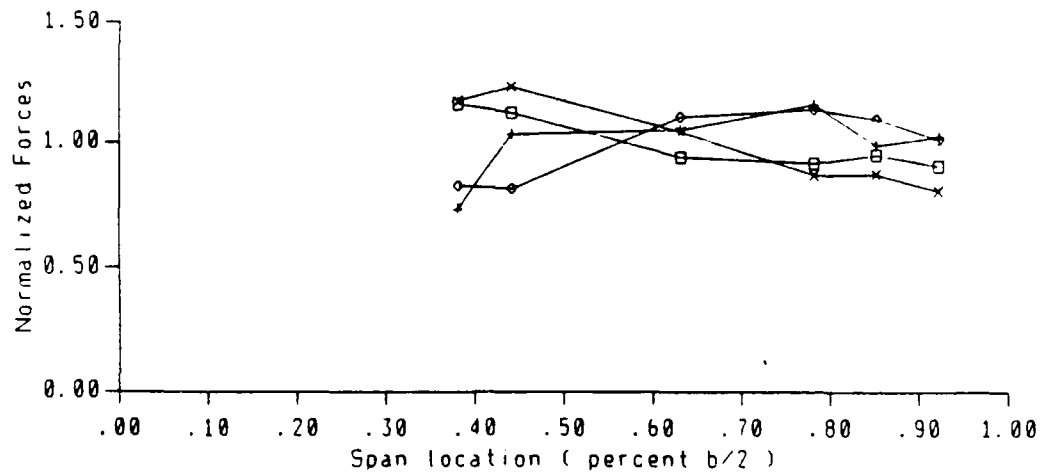
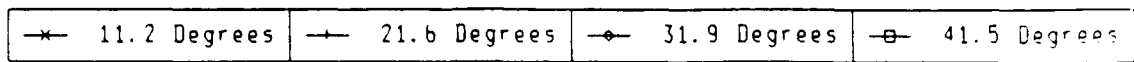
shape of the pressure force distribution is a guide to what assumed distribution might be appropriate.

Schrenk's approximation was initially used for the normal distribution above and below the pressure range. Below 11.2 degrees, C_N is approximately equal to C_L . Above 41.5 degrees, Schrenk is used because the pressure force distribution at 41.5 degrees is roughly similar.

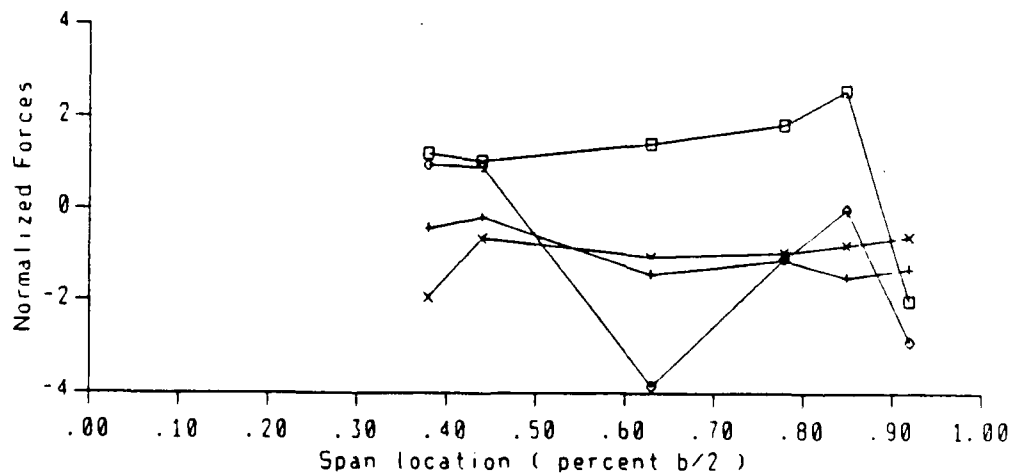
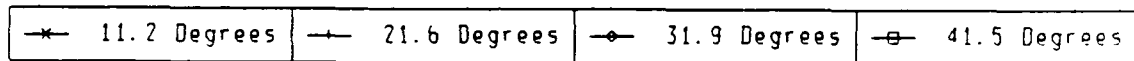
A rectangular distribution is used for axial distribution. Below 11.2 degrees, 2-d friction drag is more significant than pressure drag, and axial forces are similar by the small angle relationship. At 41.5 degrees the distribution is flat with only a slight increase (negative forward) at the wing tip.

Figure A1 shows the normal and axial pressure force distributions after normalization. The lift and drag distributions are included for reference in Figure A2. Actual forces are not shown since they are not compatible with the wind tunnel force coefficient data used throughout the angle-of-attack range of investigation (-8 to 90 degrees)⁽¹³⁾.

The wind tunnel force data is shown in Figure A3. The normal force represents a combination of a full-scale wind tunnel evaluation from -8 to 41 degrees angle-of-attack and a 1/7 scale model evaluation beyond 41 degrees. Fuselage-only data is subtracted from wing-fuselage data and the resulting wing data is corrected for fuselage blockage using a blockage factor $b.f. = 1 / (1 - (\text{blocked area} / \text{unblocked area}))$. The axial data is treated the same way.

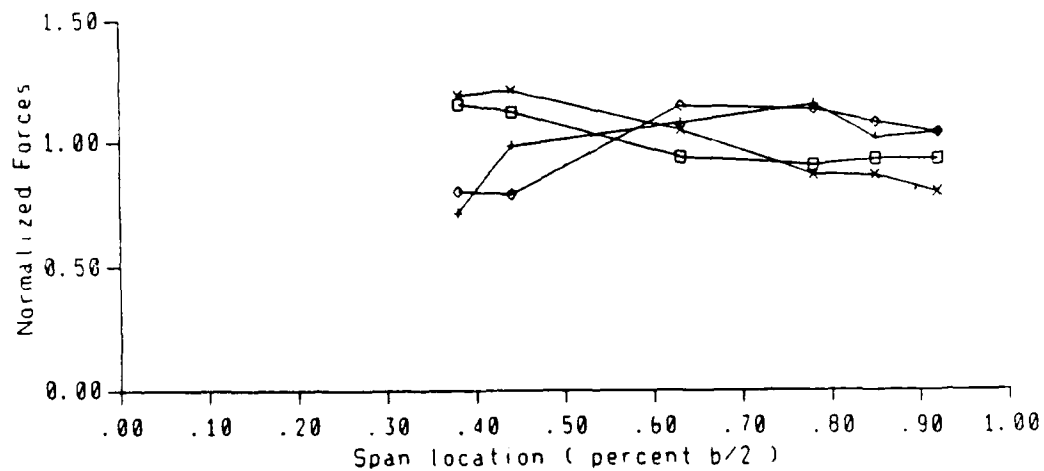
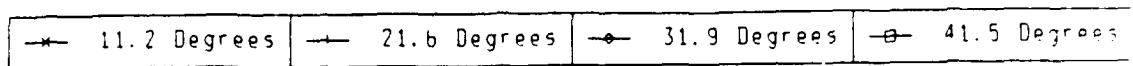


Normal Force Distribution

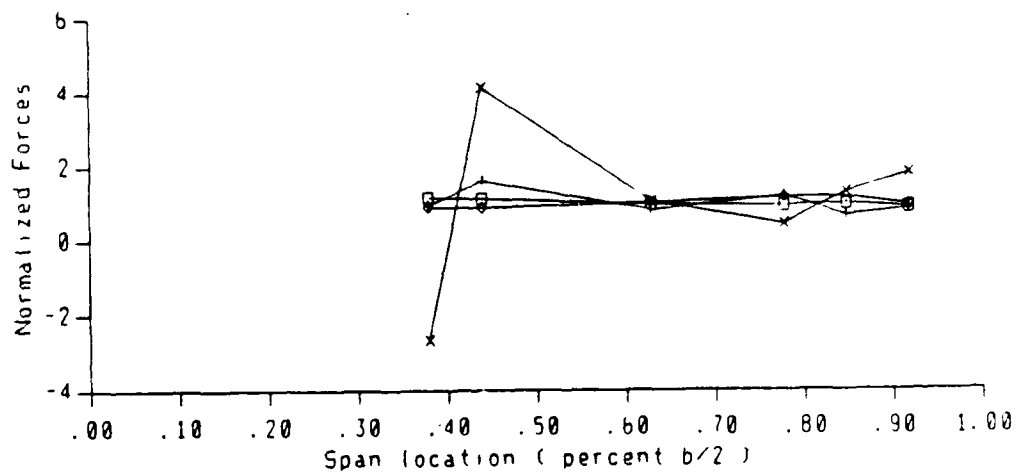
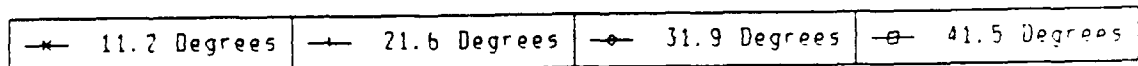


Axial Force Distribution

Figure A1: Normal and Axial Pressure Force Distributions



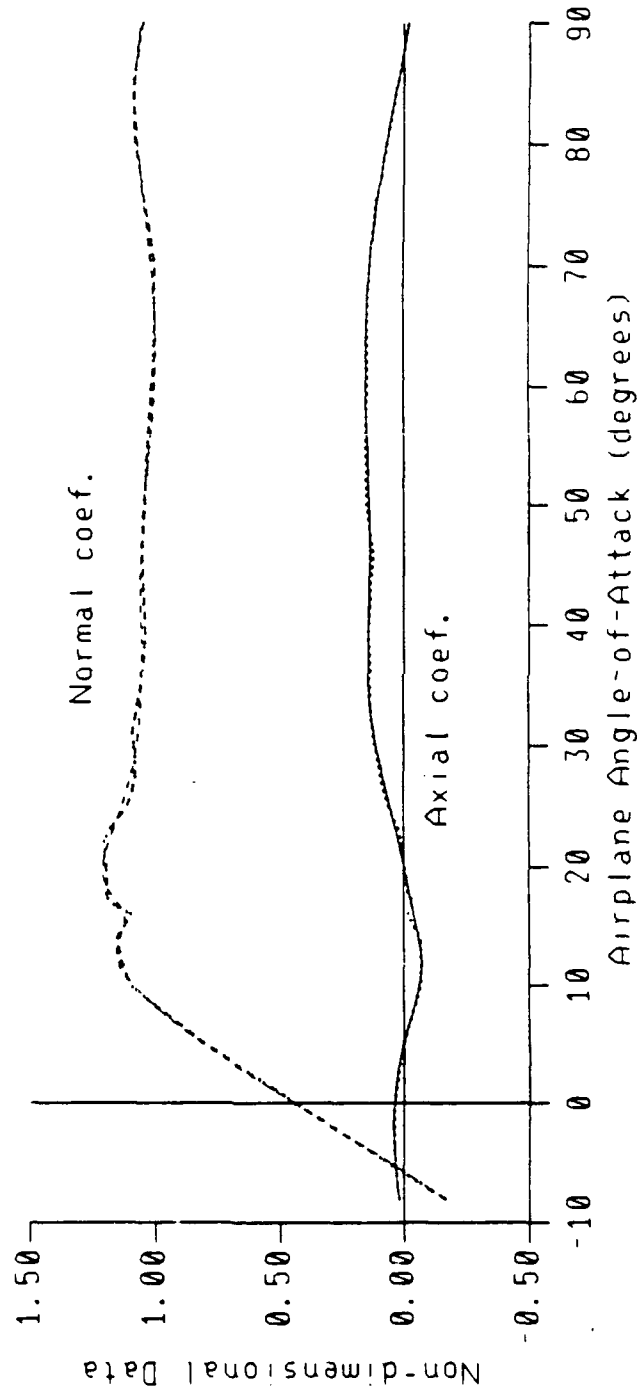
Lift Force Distribution



Drag Force Distribution

Figure A2: Lift and Drag Pressure Force Distributions

Interpolated Orig Normal Data	B-Spline Fit, Normal	Interpolated Orig Axial Data	B-Spline Fit, Axial
-----	-----	-----	-----



WIND TUNNEL FORCE COEFFICIENTS

Figure A3: Wind Tunnel Force Coefficients, Wing-Only

Appendix B: The Ritter Functions

- 1.) The Derivation of $C_l(\alpha, V, p)$ (traditionally C_{l_p} , "Damping in Roll")

$$C_l = C_l(\alpha, V, p) = -\sum_R C_{N_i} y_i \left(\frac{V_{\infty}}{V_{\infty}}\right)_i^2 d_i \frac{S_{e_i}}{S_{w_e}} + \sum_L C_{N_i} y_i \left(\frac{V_{\infty}}{V_{\infty}}\right)_i^2 d_i \frac{S_{e_i}}{S_{w_e}}$$

R and L refer to right and left wing semi-spans.

C_{N_i} is the normal force coefficient at station i,

$\frac{V_{\infty}}{V_{\infty}}$ is the local-to-freestream velocity ratio,

y_i is the moment arm from station i to the roll axis of the airplane,

d_i is the distribution factor at station i,

S_{e_i} is the effective load area for strip representation, and

S_{w_e} is the total planform wing area minus the area blocked by the fuselage and other areas not represented in the strip integration scheme.

These variables are discussed below in the order presented.

C_{N_i}

C_{N_i} is the local normal force at station i. Since C_N is a function of airplane angle-of-attack, C_{N_i} can be looked up if α_i is known. C_N of the wing is determined from three-dimensional wind tunnel data (Appendix A) and is originally distributed across the span in a uniform way. The actual spanwise strength distribution is adjusted by another factor, d_i .

Station angle-of-attack α_i is determined from the airplane angle-of-attack plus the change in angle-of-attack due to the rolling velocity, V_{roll} :

$$\alpha_i = \alpha_A + \Delta\alpha_i$$

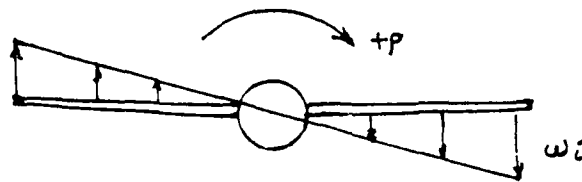
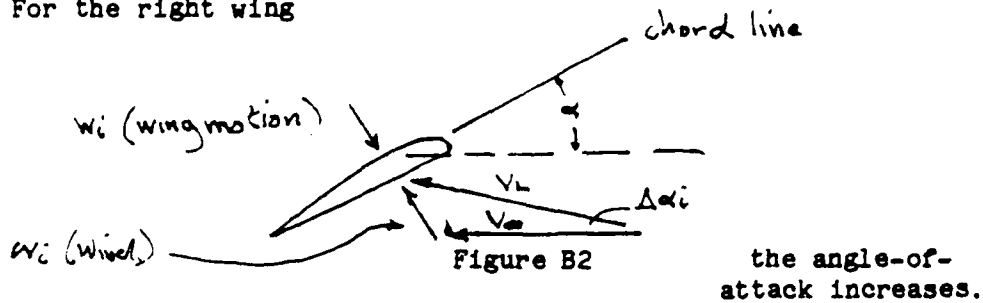


Figure B1

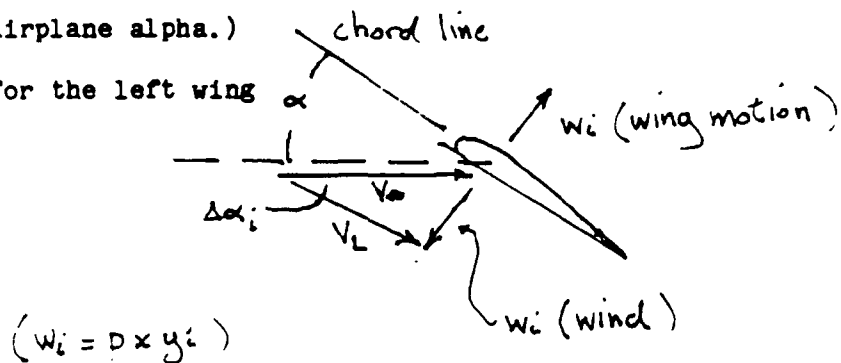
The total local velocity is affected at each point on the wing.

For the right wing



(Wing incidence is neglected since force data was evaluated at airplane alpha.)

For the left wing



$$(w_i = p \times y_i)$$

The non-rolling alpha is defined by the state variable alpha. The rolling $\Delta\alpha_i$ is defined by the state variables V_{ω} and p as follows:

Right wing:

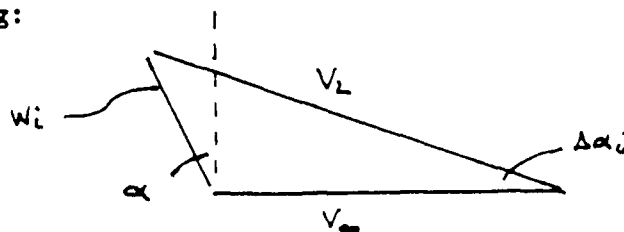
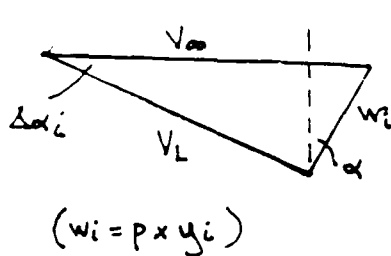


Figure B4

Using the law of sines, $\frac{\sin \Delta\alpha_i}{p y_i} = \frac{\sin (90^\circ - \alpha - \Delta\alpha_i)}{V_\infty}$

and through trig. identities, $\Delta\alpha_i = \tan^{-1} \left[\frac{p y_i \cos \alpha}{V_\infty + p y_i \sin \alpha} \right]$

Similarly for the left wing:



$$\Delta\alpha_i = \tan^{-1} \left[\frac{p y_i \cos \alpha}{V_\infty - p y_i \sin \alpha} \right]$$

($w_i = p x y_i$)

Figure B5

It can be shown that these equations are valid for positive and negative combinations of roll and yaw. It only necessary to remember that for the left wing, $\alpha'_i = \alpha_A - \Delta\alpha_i$

The most effective way to define C_N vs. α within the program is from a table of values. This means digitizing of the appropriate curves from reference 5. This was done by selecting a few critical points and fitting a cubic spline to them. Graphic comparisons are made to insure a smooth and satisfactory fit (Appendix A). The ensuing table of cubics is initiated into an array in a program used to evaluate the derivatives. As conditions are encountered, the table can be read and interpolated as required.

Since it is the local dynamic pressure that accounts for the actual forces ($F_n = C_n q S$) the ratio of local pressure to freestream pressure is required: $\frac{q_L}{q_\infty} = \frac{\frac{1}{2} \rho_L V_L^2}{\frac{1}{2} \rho_\infty V_\infty^2}$

For the conditions investigated $\rho_L = \rho_\infty$ so it is the ratio of velocities that is all that needs to be considered. For velocity ratio expressions, it is better to use the law of cosines, thus avoiding singularities possible with the law of sines. The following expression has been shown to be valid for all combinations of roll rate and angle-of-attack.

$$\left(\frac{V_L}{V_\infty}\right)^2 = 1 + \frac{py_i (py_i + 2V_\infty \sin \alpha)}{V_\infty^2}$$

For the left wing, the second sign in the expression is changed. The velocity ratio for the left wing, positive alpha, positive roll, is seen to be less than one.

y_1 (non-dimensional)

The pressure tests of reference 6 were conducted at semi-span locations $2y/b = .38, .44, .63, .78, .85$, and $.92$. These values are adopted for this analysis. Actual lengths are used in the scalar approach of the preceding derivations.

d_1 (non-dimensional)

These factors represent the spanwise distribution across the effective use area of the wing (next paragraph). All distributions have been normalized to have a mean value of one (Appendix A.)

Se_1 , Effective Load Area for Integration

Forces on the wing cause moments about the axis of rotation. To get a fair calculation, at least the outer one-half of each

wing panel must be considered. Rather than interpolating a uniformly distributed array of span locations to be evaluated at uniform areas, the selected pressure regions are used with areas defined within shared boundaries.

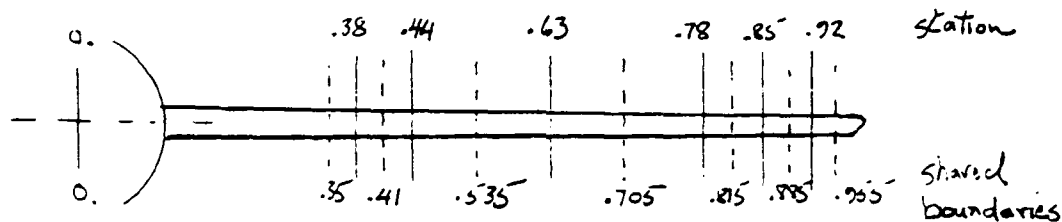


Figure B6

	①	②	③	④	⑤
i	y_i	$\frac{1}{2}(\textcircled{1}_i - \textcircled{1}_{i+1})$	$\textcircled{1}_i + \textcircled{2}_{i-1}$	$\textcircled{3}_i - \textcircled{3}_{i+1}$ $+ 12.25 \times \frac{1}{2}$	$\textcircled{4}_i \div \Sigma \textcircled{4}_i$
1	.92	.035	.955	3.43	.116
2	.85	.035	.885	3.43	.116
3	.78	.075	.815	5.39	.182
4	.63	.095	.705	8.33	.281
5	.44	.03	.535	6.125	.207
6	.38	(-.03)	.410	2.95	.099
			.350		

Table B1

Column ① values are normalized wing stations ($b/2 = 1$).

Column ② values are half the distance between stations.

Column ③ values are shared boundary stations.

Column ④ values are actual areas associated with station i locations, S_{e_i} . S_{w_e} is the sum of column ④ values in Table B1. $S_{w_e} = 29.65 \text{ ft}^2$.

Column ⑤ values are normalized area ratios S_{e_i}/S_{w_e} .

The Rolling Moment

The total moment is evaluated as follows:

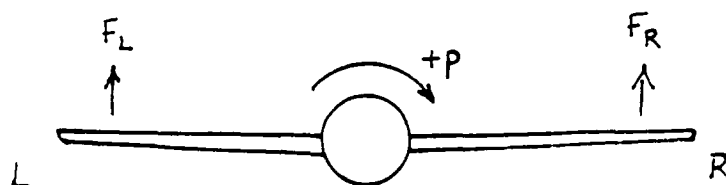


Figure B7

When p is positive, F_R will produce a negative moment and F_L a positive moment. When the airplane is flying much below stall, F_R will be greater than F_L and the net moment due to rolling will be negative (stabilizing).

The product of force and moment arm coefficients, with the necessary adjustment coefficients for dynamic pressure, area and distribution, give the total moment coefficient evaluated for each wing panel, left and right. The sum of left and right total moments gives a net rolling moment due to rolling coefficient:

$$C_l(\alpha, V, p) = -\sum_R C_{N_i} y_i \left(\frac{V_i}{V_\infty}\right)_i^2 d_i \frac{S_{e_i}}{S_{w_e}} + \sum_L C_{N_i} y_i \left(\frac{V_i}{V_\infty}\right)_i^2 d_i \frac{S_{e_i}}{S_{w_e}}$$

An artificial derivative C_{l_p} can be constructed for the purpose of comparing Ritter functions with Bihle derivatives, i.e., $C_{l_p} = C_l/p$ where p is non-zero. When used as a subroutine in the spin integration program, it is only the moment itself that is required, so conditions of zero roll rate do not present the problem of indefinable equations. When the subroutine is used independently as a research tool the roll conditions are controlled to avoid the problem.

The following page describes the different configurations for angle-of-attack and rolling motion.

Right wing, positive alpha, positive roll rate:

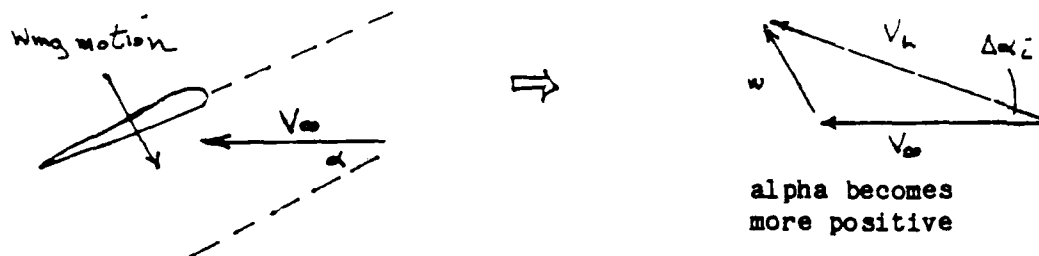


Figure B8

Right wing, negative alpha, positive roll rate:

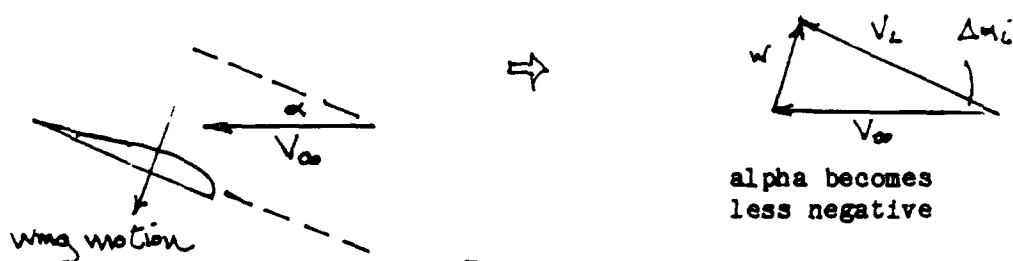


Figure B9

Right wing, positive alpha, negative roll rate:

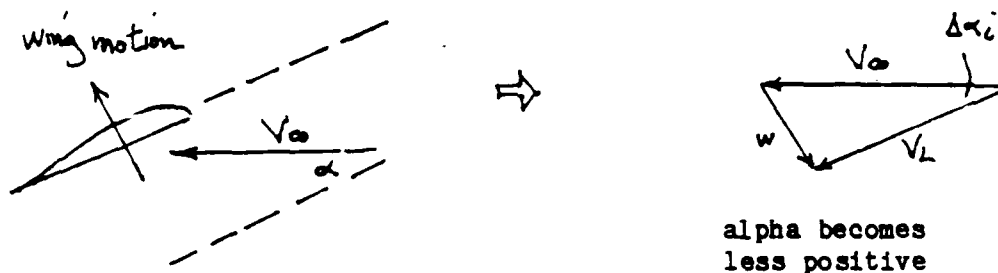


Figure B10

Right wing, negative alpha, negative roll rate:



Figure B11

2.) The Derivation of $C_l(\alpha, V, r)$ (traditionally C_{l_r} , Roll Moment Due to Yaw Motion)

The correct equations are derived from the following diagrams in a manner similar to the derivations in Part 1.) of this Appendix.

Right wing, positive alpha, positive yaw rate:

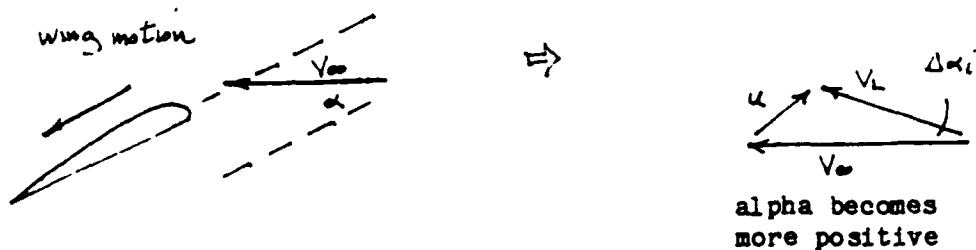


Figure B12

Right wing, negative alpha, positive yaw rate:

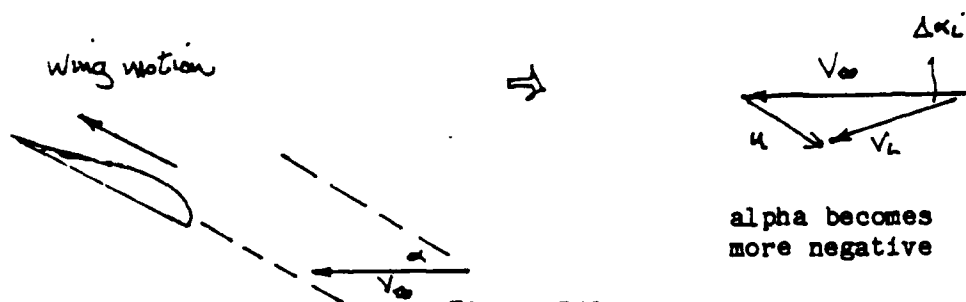


Figure B13

Right wing, positive alpha, negative yaw rate:

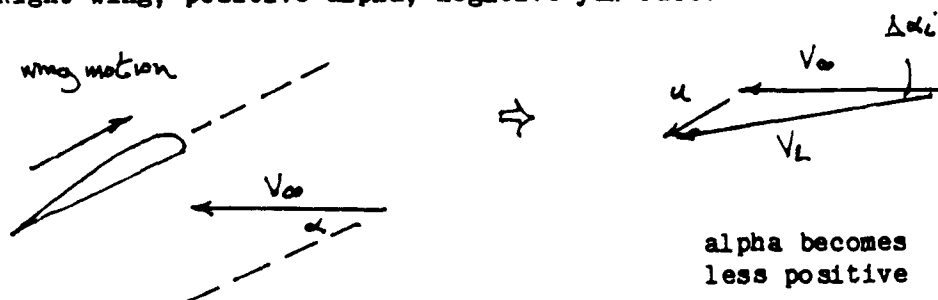


Figure B14

Right wing, negative alpha, negative yaw rate:

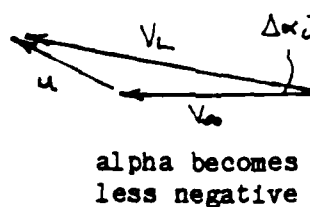
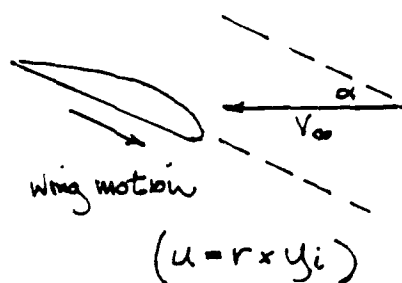


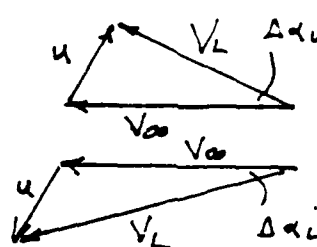
Figure B15

$$\Delta \alpha_i = \tan^{-1} \left[\frac{u \sin \alpha}{V_\infty - u \cos \alpha} \right]$$

$$\Delta \alpha_i = \tan^{-1} \left[\frac{u \sin \alpha}{V_\infty + u \cos \alpha} \right]$$

$$\alpha_i = \alpha + \Delta \alpha_i$$

$$\alpha_i = \alpha - \Delta \alpha_i \text{ (Left wing)}$$



Only the first expression above is required to evaluate all combinations of r and α for the right wing.

$$C_l = C_l(\alpha, V, r) = -\sum_R C_{N_i} y_i \left(\frac{V_L}{V_\infty} \right)_i^2 d_i \frac{S_{c_i}}{S_{w_c}} + \sum_L C_{N_i} y_i \left(\frac{V_L}{V_\infty} \right)_i^2 d_i \frac{S_{c_i}}{S_{w_c}}$$

3.) The Derivation of $C_n(\alpha, V, p)$ (traditionally C_{n_p} , Yaw Moment Due to Roll Motion)

C_{n_p} differs from C_{l_p} and C_{l_r} in that axial force data is used to calculate the net moment. C_A of the wing is determined by subtracting C_A body wind tunnel data from C_A wing-body data. The resulting curve is seen to be negative (thrusting) between 5 and 21 degrees alpha (Appendix A).

$$C_n = C_n(\alpha, V, p) = \sum_R C_{A_i} y_i \left(\frac{V_{\infty}}{V_p}\right)_i^2 d_i \frac{S_{ei}}{S_{we}} - \sum_L C_{A_i} y_i \left(\frac{V_{\infty}}{V_p}\right)_i^2 d_i \frac{S_{ei}}{S_{we}}$$

4.) The Derivation of $C_n(\alpha, V, r)$ (traditionally C_{n_r} ,
"Damping in Yaw")

For both C_{n_p} and C_{n_r} , caution must be used in interpreting data. As seen in Appendix A, drag is always positive (rearward) but the axial force distribution is quite variable in polarity.

$$C_n = C_n(\alpha, V, r) = \sum_R C_{n_i} y_i \left(\frac{V_L}{V_\infty}\right)_i^2 d_i \frac{S_{wi}}{S_{wc}} - \sum_L C_{n_i} y_i \left(\frac{V_L}{V_\infty}\right)_i^2 d_i \frac{S_{wi}}{S_{wc}}$$

Appendix C: Bihrlle Derivatives and Ritter Functions Compared

The following charts reflect direct evaluation of the Wykes equations and conditional evaluation of the Ritter equations. Baseline conditions for evaluation of the Ritter equations are, velocity is 120 feet per second and roll and yaw rates are both one radian per second.

The Bihrlle derivatives for the subject airplane are reproduced from the report⁽¹⁴⁾ and shown in Figure C1. The Ritter baseline evaluations are displayed in Figure C2.

Because the Ritter equations are dependent on more than one flight parameter, they can only be conditionally displayed. The following pages show the variations in the functions resulting from different velocities (Figure C3) and from different roll and yaw rates (Figure C4).

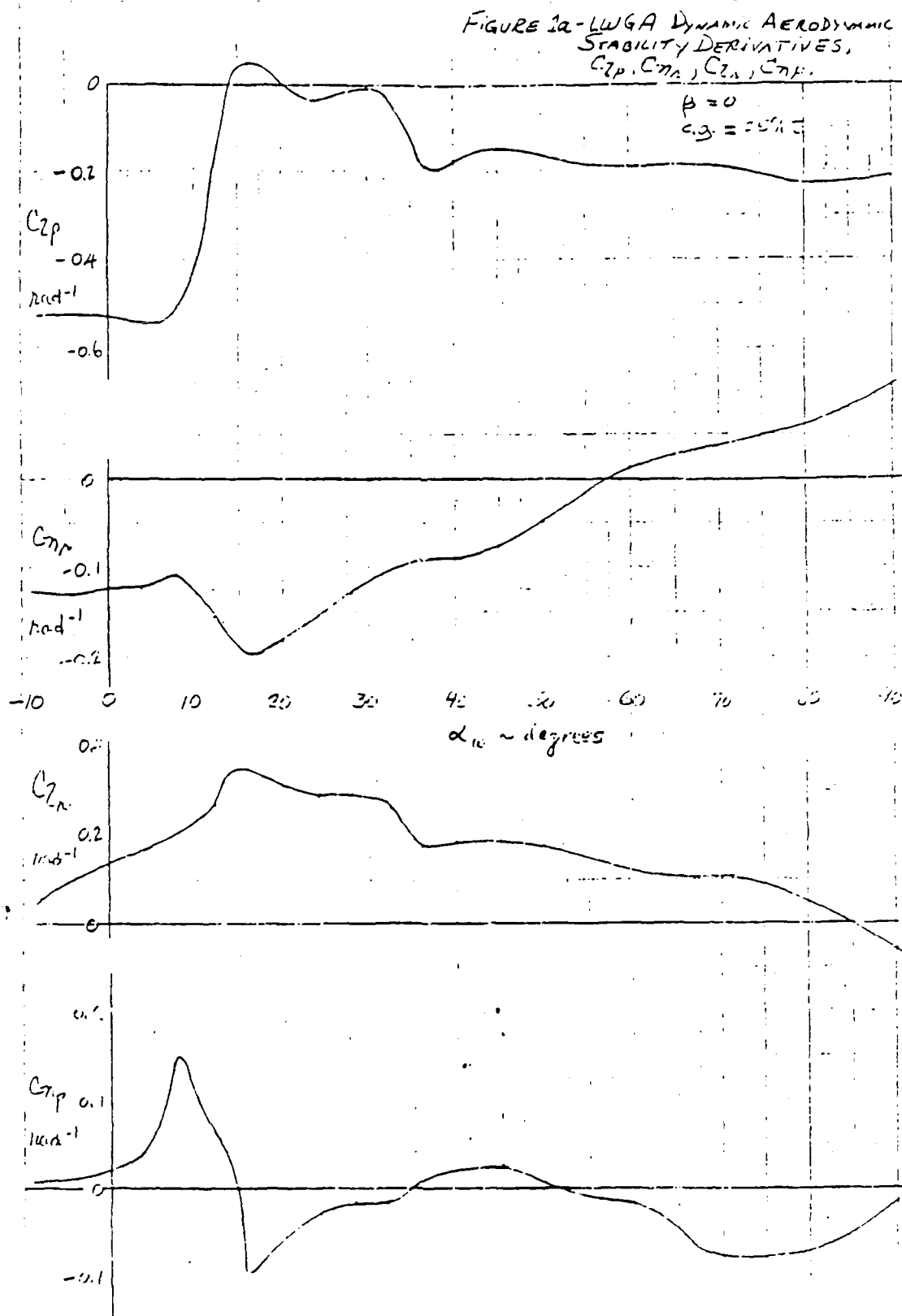
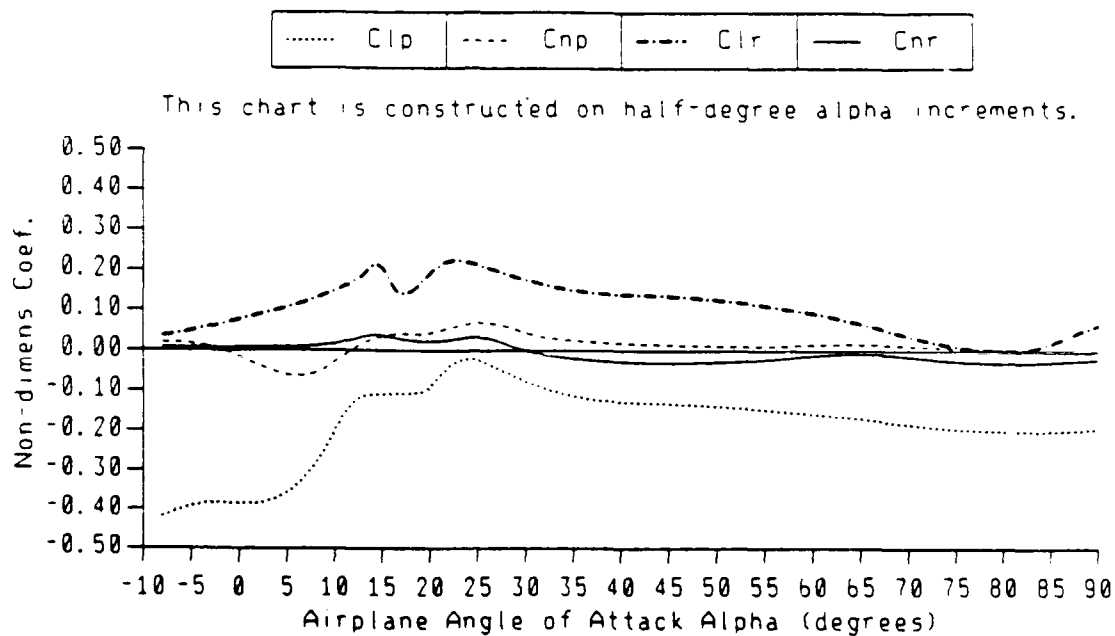
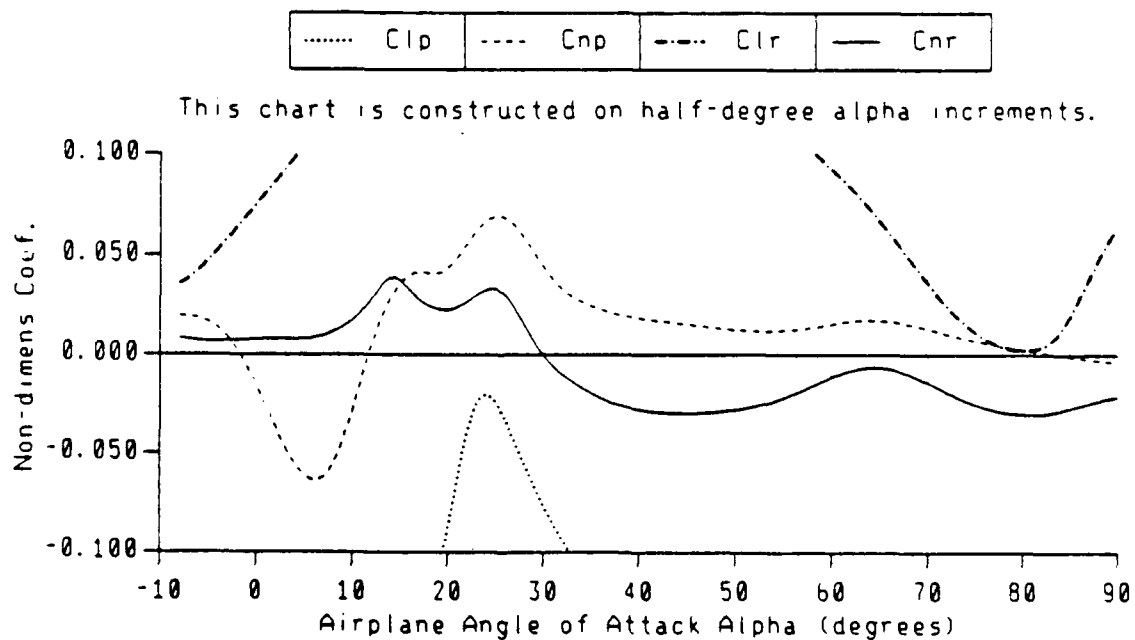


Figure C1: The Bihrie Derivatives



Ritter derivatives, $V/120^\circ$, $\text{Beta}/0^\circ$, $P/1^\circ$, $R/1^\circ$

Figure C2a: Baseline Ritter Functions



Ritter derivatives, $V/120^\circ$, $\text{Beta}/0^\circ$, $P/1^\circ$, $R/1^\circ$

Figure C2b: Baseline Ritter Functions, Reduced Scale

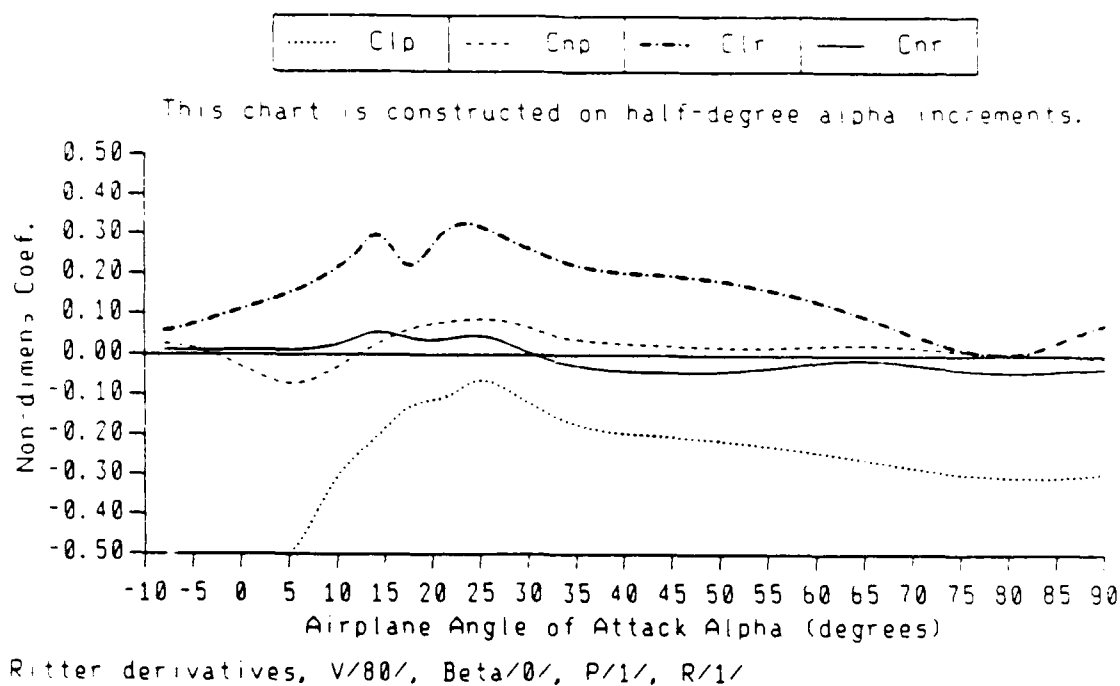


Figure C3a: The Ritter Functions, $V = 80$ ft/sec

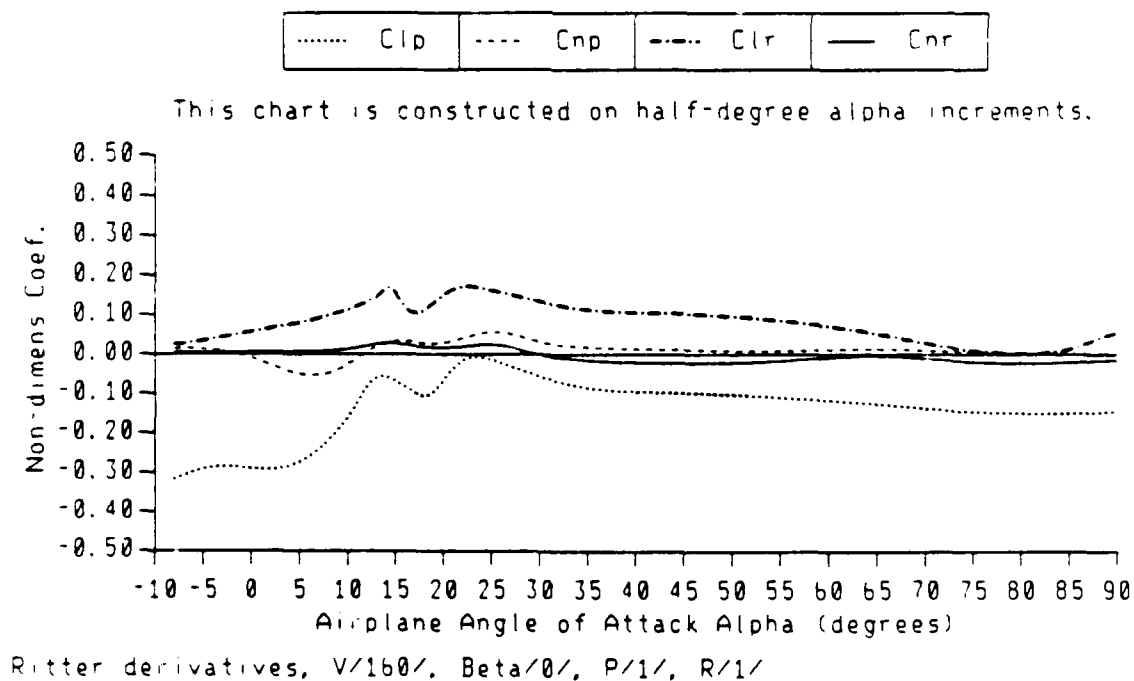
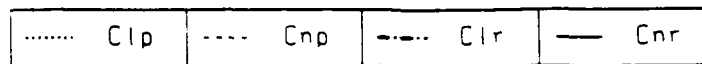
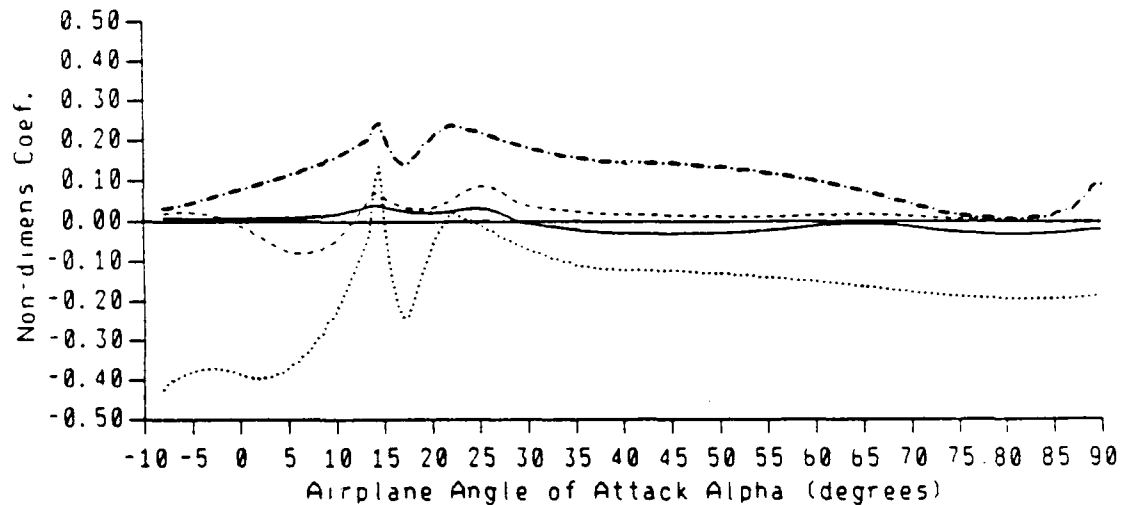


Figure C3b: The Ritter Functions, $V = 160$ ft/sec

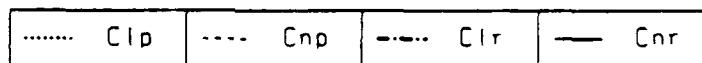


This chart is constructed on half-degree alpha increments.

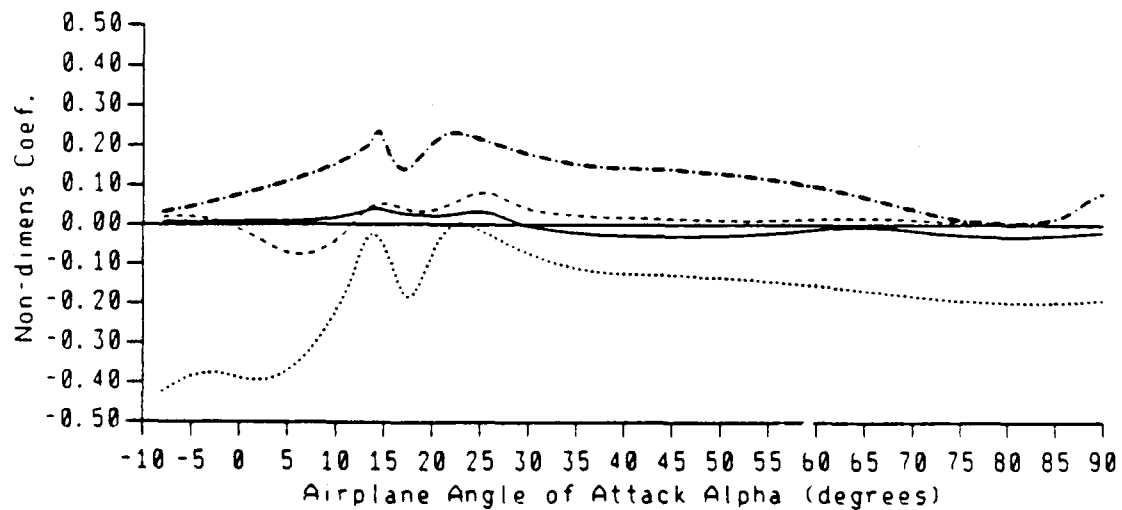


Ritter derivatives, $V/120^\circ$, $\text{Beta}/0^\circ$, $P/.1^\circ$, $R/.1^\circ$

Figure C4a: The Ritter Functions, p and $r = .1$ rad/sec

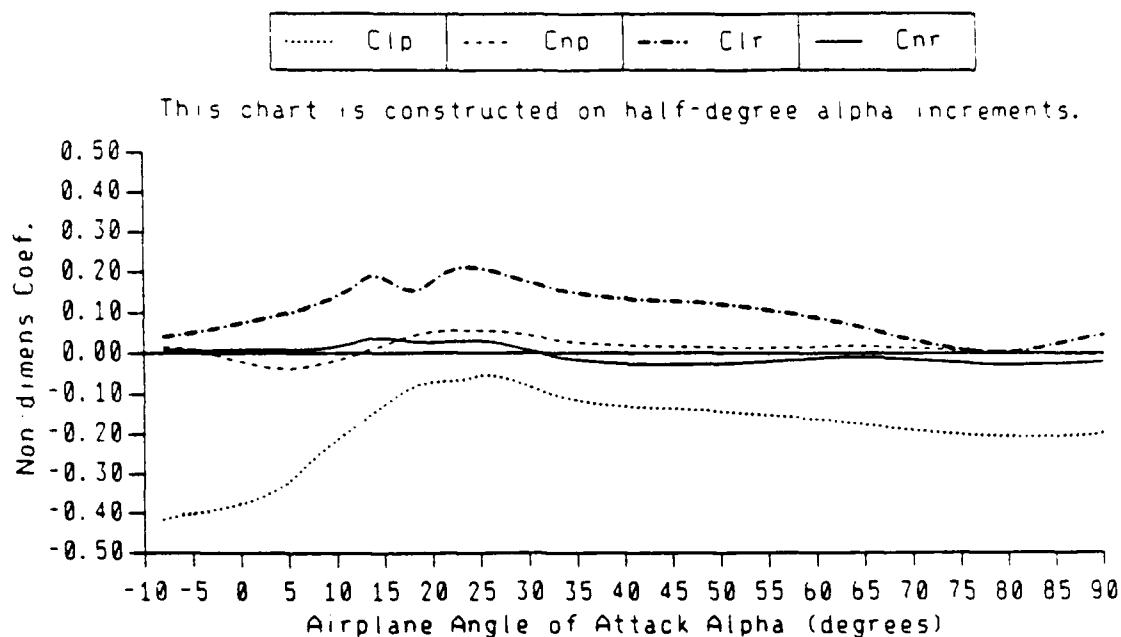


This chart is constructed on half-degree alpha increments.



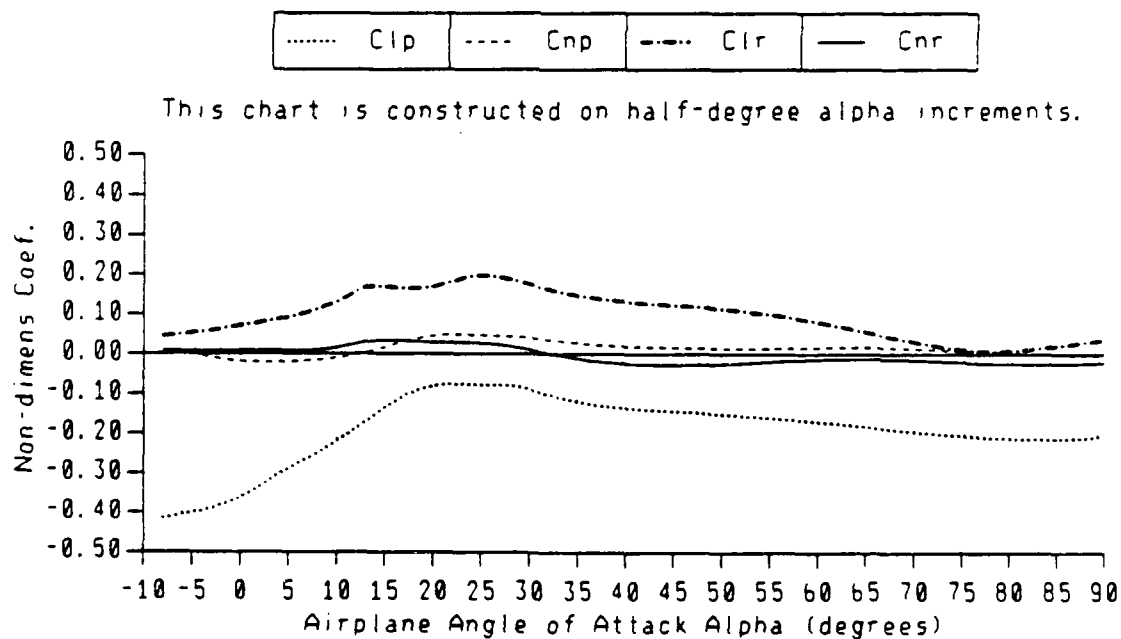
Ritter derivatives, $V/120^\circ$, $\text{Beta}/0^\circ$, $P/.5^\circ$, $R/.5^\circ$

Figure C4b: The Ritter Functions, p and $r = .5$ rad/sec



Ritter derivatives, $V/120\%$, $\text{Beta}/0\%$, $P/1.8\%$, $R/1.8\%$

Figure C4c: The Ritter Functions, p and $r = 1.8$ rad/sec



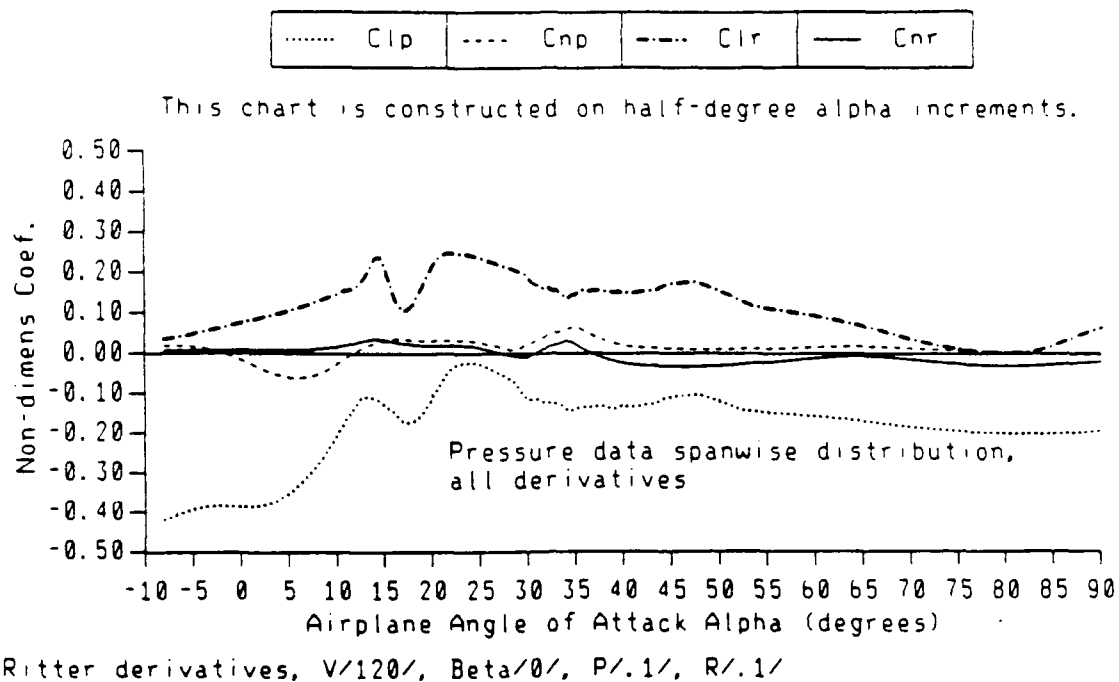
Ritter derivatives, $V/120\%$, $\text{Beta}/0\%$, $P/2.5\%$, $R/2.5\%$

Figure C4d: The Ritter Functions, p and $r = 2.5$ rad/sec

Appendix D: Sensitivity to Spanwise Force Distribution

A conditional set of Ritter "derivatives" ($V = 120$ ft/sec, p and $r =$ one rad/sec) were evaluated for different spanwise distributions.

The original research distribution (Schrenk for normal forces, rectangular for axial) is used to derive the rate derivatives shown in Figure C2 of Appendix C. The pressure distribution described in Appendix A is applied in computing the derivatives shown in Figure D1. The Schrenk distribution is applied for all derivatives in Figure D2 and the rectangular distribution is applied for all derivatives in Figure D3.



**Figure D1a: Baseline Ritter Functions
Pressure Force Distribution**

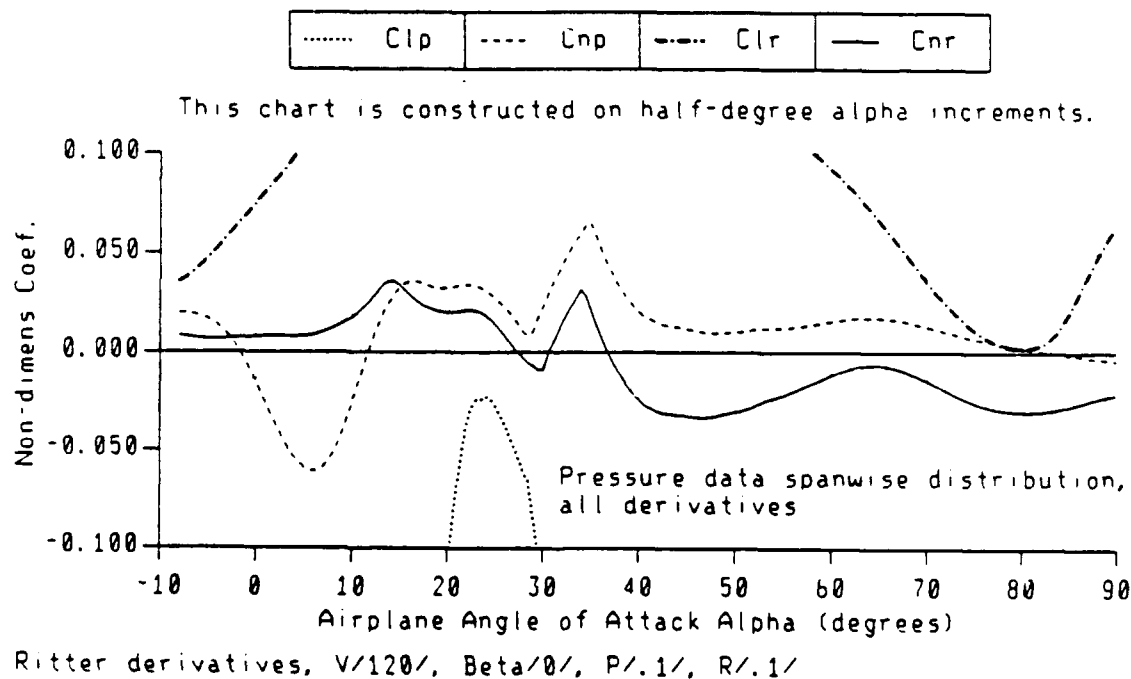


**Figure D1b: Baseline Ritter Functions, Reduced Scale
Pressure Force Distribution**

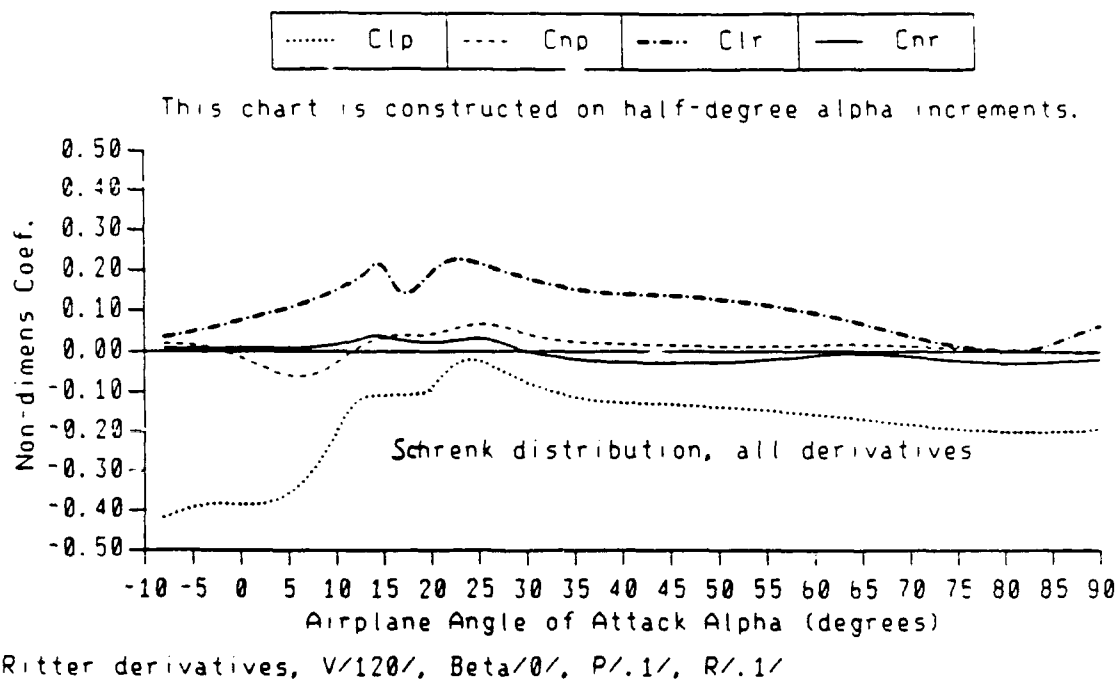


**Figure D2a: Baseline Ritter Functions
Schrenk Distribution**

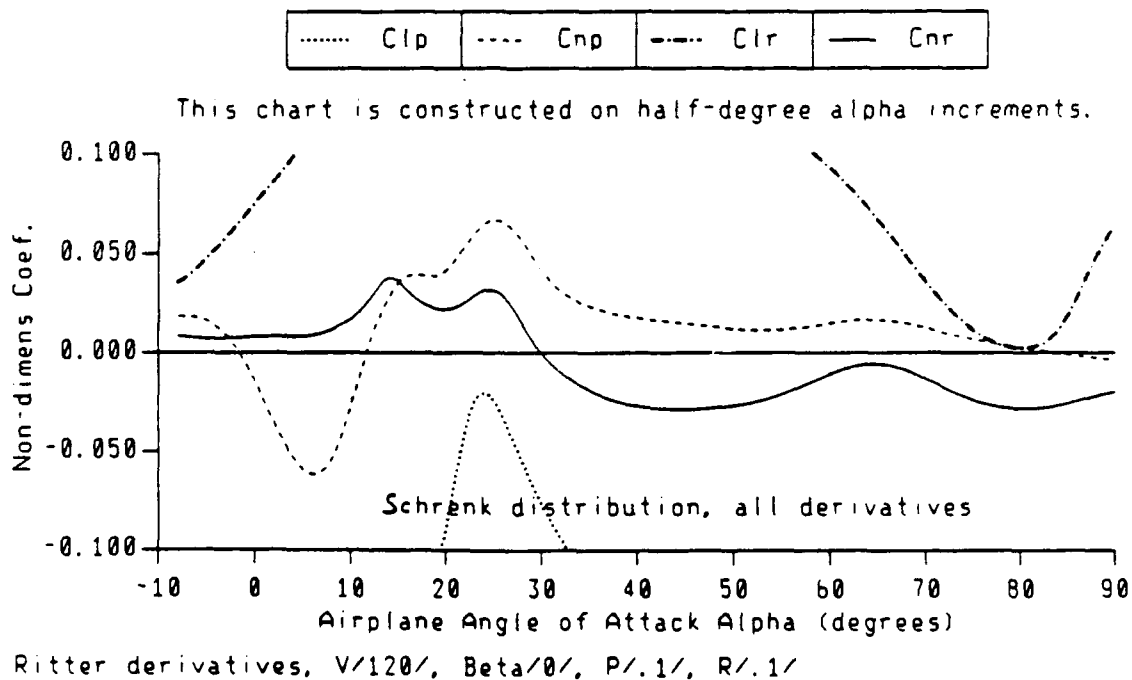


**Figure D2b: Baseline Ritter Functions, Reduced Scale
Schrenk Distribution**

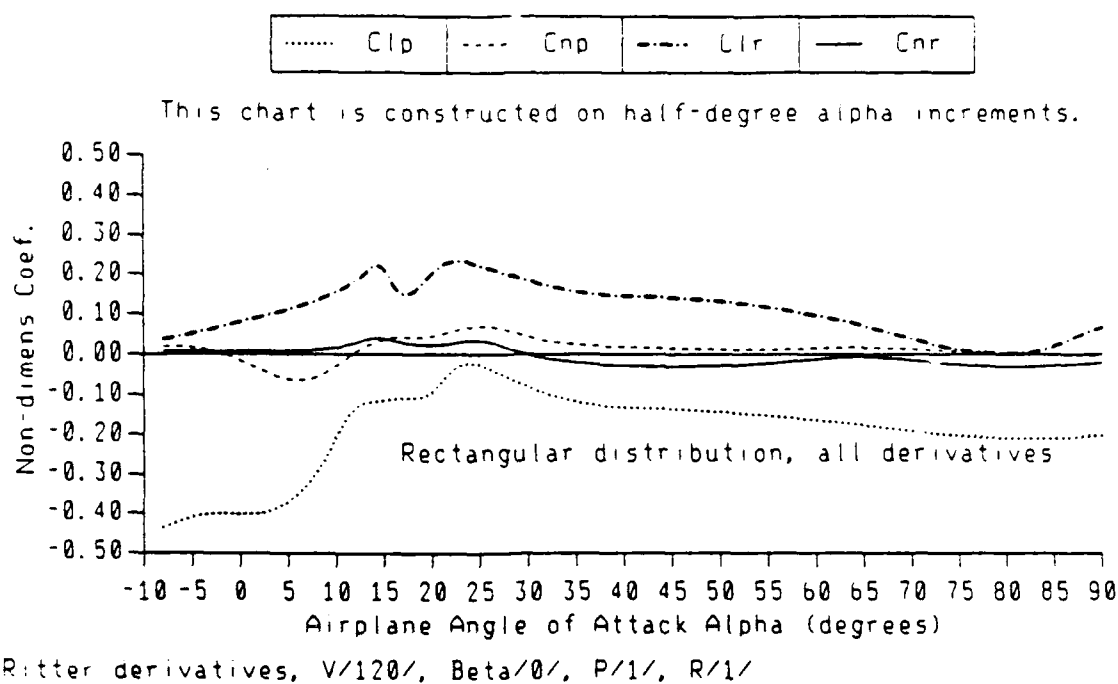


**Figure D3a: Baseline Ritter Functions
Rectangular Distribution**

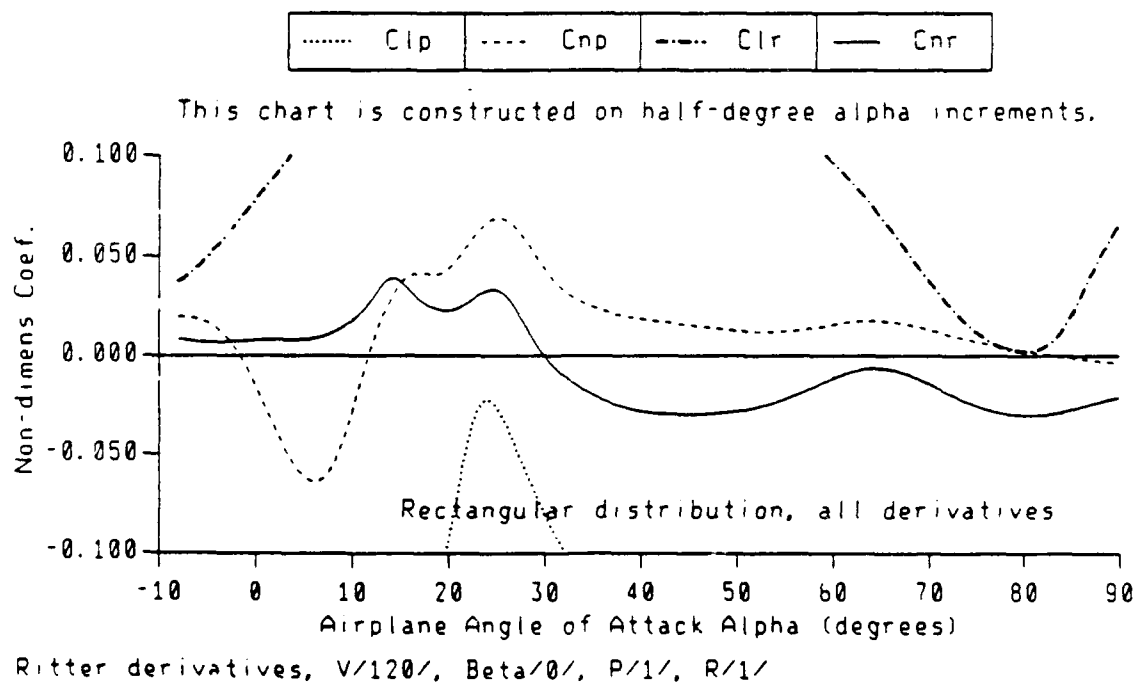


**Figure D3b: Baseline Ritter Functions, Reduced Scale
Rectangular Distribution**

APPENDIX B

PREDICTION OF PLANFORM MODIFICATION EFFECTS AT HIGH ANGLES OF ATTACK

M.G. Nagati* and B. Rashidian**
The Wichita State University
Wichita, Kansas

Abstract

A method is presented for the estimation of the effects of wing planform modifications on its aerodynamic forces using the popular panel methods. The objective of such estimation is to assist in the preliminary concept design of spin resistant aircraft. The pressure distributions are obtained by applying changes to the boundary conditions at the panel control points to simulate separated boundary layer flow. The changes in normal velocity vectors are computed based on 2-dimensional airfoil data beyond the onset of separation. Results for angles of attack up to 27° are in agreement with the experiment. Another run at a 32° angle of attack shows a deviation from experimental data, however, the error is the same for the baseline and the planform modification considered.

Nomenclature

b	wing span
$C_l(y)$	local lift coefficient at a wing section at a span location y
C_l	lift curve slope in the linear range
C_p	pressure coefficient
L, M, N	aerodynamic rolling, pitching and yawing moments
n	normal vector to surface
P, Q, R	roll, pitch and yaw rates
V	velocity vector
x	chordwise distance from leading edge
y	distance from the plane of symmetry
y'	non-dimensional $y = 2y/b$
α_0	angle of attack of the entire wing
$\alpha(y)$	local angle of attack at a span location y
Γ	bound filament vortex strength
σ_i	source strength for panel i

Subscripts

i or j	panel or section number
n	normal component
l.l.	limit of linear range of C_l
sep	separation point on airfoil
σ	induced due to singularities
∞	free stream

Introduction

The stall/spin characteristics of general aviation aircraft have been the subject of renewed interest in recent years. Flight safety considerations have led to a thorough flight test and other experimental programs at NASA-Langley and a number of universities.

Spin entry results at high angles of attack due to the resulting adverse rates of change of aerodynamic moments with respect to angular velocities of the aircraft. These moments are caused mainly

by surface pressure distributions on the wing, but other surfaces trailing it (fuselage tailcone and stabilizer surfaces) are also involved. Even though their contribution is very important, these other surface effects are caused by the wing wake which becomes unsymmetric upon spin entry. Therefore, much of the spin research concentrates on wing character at high angles of attack.

In designing spin-resistant aircraft configurations, a preliminary step is to examine the lift coefficient vs. angle of attack curve beyond stall. A sharp drop in lift with increasing α indicates the potential for unfavorable rolling moment rate of change with roll rate ($\partial L / \partial P$). A strip (or preferably surface) integration of the moments of normal and axial forces along the wing span is necessary for a more conclusive evaluation of wing character, since the effective angle of attack varies with spanwise location^{1,2}.

For a configuration to be spin resistant, or at least to enter the spin gently, the wing planform must be such that the post-stall behavior of its outboard panels is mild (the outboard panels are more critical due to their larger moment arm). This is illustrated in Figure 1.

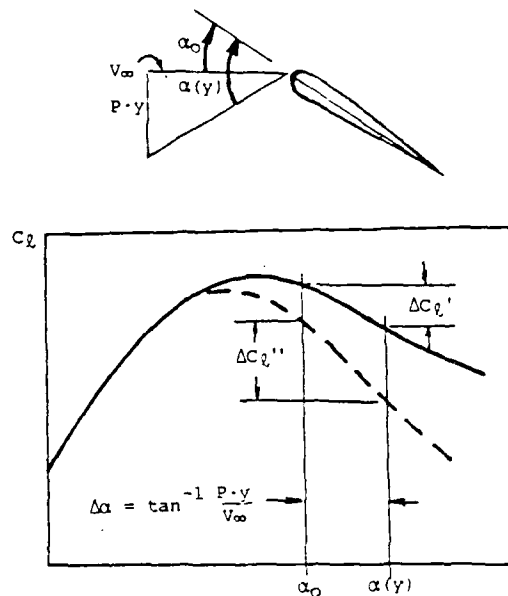


Figure 1. Effect of local α on lift and hence rolling moment.

In order to achieve this design objective, an outboard panel leading edge cuff (extension) was developed and tested at NASA-Langley³. It was also adopted for at least one recent general aviation design. The abrupt change in chord length and leading edge camber causes a delay in the stall of the outboard panel which provides the desired spin character. Reference 3 shows oil flow visualiza-

*Associate Professor, Aeronautical Engineering Dept., Associate of the Institute for Aviation Research. Senior member AIAA.

**Graduate student

tions of an aircraft wing with and without the leading edge device near and beyond C_{lmax} . The oil flow photographs clearly show the outboard panel remaining attached for the modified wing.

The objective of the present work is to enable computational prediction of this behavior in order to provide preliminary designers with a capability to evaluate planform modifications.

The method, which is in its early stages of development, is based on a special application of potential flow (panel) methods to simulate separated flow. The idea is to artificially generate a boundary layer effect by altering the surface boundary condition in the solution of Laplace's equation. Panel methods solve this equation by enforcing boundary conditions of zero flow across solid boundaries. In order to simulate the boundary layer, a nonzero normal velocity distribution on the separated portions of the wing surface is specified as boundary condition.

The method presented is simple, requires minor modifications to existing potential flow codes with which many aerodynamic configuration designers are familiar. It provides good estimates of the change in character due to planform modifications.

Background

Nature of the Airflow Around a Cuffed Wing

Following the success of the leading edge cuff design and the results of its oil flow aerodynamic evaluation, a detailed study [4] was conducted at the Wichita State University wind tunnel facility to understand the mechanism of delaying separation on the outboard panel of such a wing.

In this study, velocity and pressure data were obtained with a five tube pressure sensing probe. Measurements in the flow field above and behind the wing upper surface were taken so that: a) vorticity could be detected, and b) the separated wake could be determined.

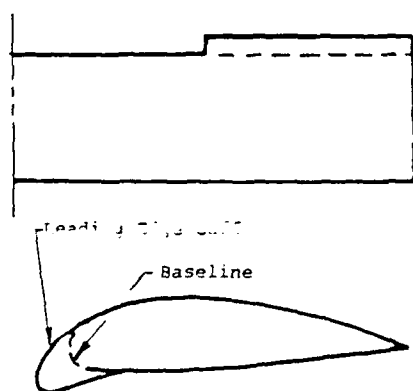


Figure 2. Cuffed wing configuration.

This investigation led to the following conclusions:

1. The sudden change in chord at the notch leads to a change in bound vorticity (see figure 2).
2. In addition, especially at high α , the peak negative pressure near the leading edge is much lower outboard of the notch due to the droop.
3. The combined effect of the above leads to the shedding of a strong vortex from the leading edge.

4. This vortex interacts with the tip vortex and is pulled toward the tip, introducing energy into the boundary layer and reducing its thickness considerably.

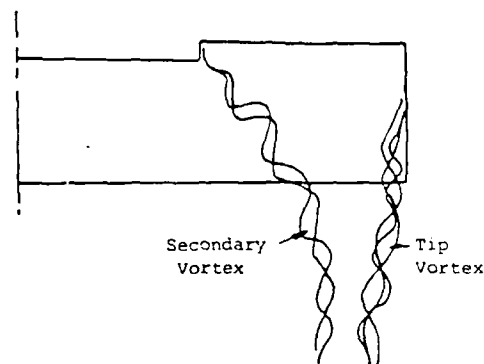


Figure 3. Vortex Interaction.

5. The flow does not really remain attached on the outboard panel, but is less gravely separated with the introduction of the cuff.

Computational Model

In the present work, the separated flow is modeled only by modifying the boundary condition of the potential flow panels. No attempt was made to account for the interaction of the two trailing vortices. This would require an iterative (relaxation) scheme. Also, the vortex sheet is left on the surface of the wing. A more realistic model would allow for its displacement away from the surface in the separated regions. The normal velocities used to modify the panel boundary conditions to simulate a boundary layer are computed for chordwise 2-D airfoil sections. In that model, a single vortex filament at the quarter chord is used rather than a distributed vortex sheet and crossflows are not accounted for. These simplifying assumptions lead to some estimation error, but adequately allow prediction of the incremental effects of small changes in planform.

Description of the Method

The computation is performed in the following sequence:

- a) A 3-D potential flow analysis is performed on the wing at the desired angle of attack with no simulated separation. The objective is to obtain an initial $C_l(y)$ distribution by strip integration of the local pressure coefficients (Figure 4a).

- b) The flow is assumed strictly chordwise. For each section i (located at y_i), a local angle of attack $\alpha(y_i)$ is obtained which corresponds to $C_l(y_i)$ by solving the equation of the linear portion of the lift curve (the dashed line in Figure 4b), where the slope is $C_{l\alpha}$. This local $\alpha(y)$ is an initial estimate of the finite span effect of the wing at the local section.

- c) If the flow is separated at the section in question (i.e. if the local α exceeds the linear limit $\alpha_{l.l}$, then $C_l(y_i)$ is read from Figure 4b (solid line) as well as x_{sep} and C_{psep} (Figure 4c). These three values must be available from 2-D air-

foil data (experimental or computational).

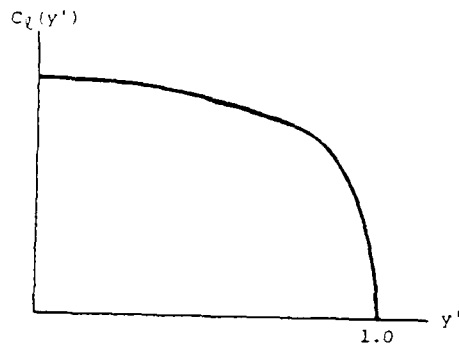
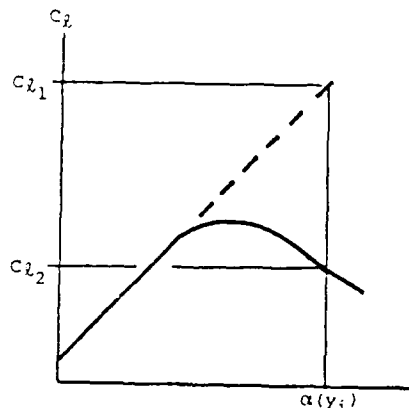


Figure 4a. Potential flow spanwise lift distribution



C_{l1} = Potential Flow C_l at y_i
 C_{l2} = Required for $\alpha(y_i)$

Figure 4b. Airfoil lift curve

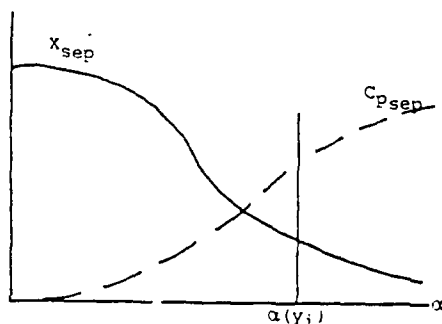


Figure 4c. Required separation data for local airfoil section

d) The assumption is made that the pressure coefficient remains constant downstream of the separation point. The problem now is to "design" the circulation and the boundary conditions for the airfoil section, namely V_{ni} for each control panel on the separated flow surface so that:

1. The lift coefficient is equal to the finite wing local $c_l(y_i)$ and,

2. The pressure coefficient at all panel control points downstream of the separation point is equal to C_{psep} corresponding to α_i .

This is performed iteratively by using a function minimization technique (steepest decent). The problem is then:

$$\text{minimize } f = K[C_l - c_l(y_i)]^2 + \sum_{j: x_j > x_{sep}} [C_{pj} - C_{psep}]^2$$

where C_l and C_{pj} are functions of the design variables Γ , V_{nj} . They are computed for each variation of these design variables.

The function f represents the difference between the desired separated pressure distributions and lift coefficient and the ones resulting from the computations. C_l and C_{pj} are computed using a 2-D panel program which features a single vortex of strength Γ at the aerodynamic center and constant source panels. The panel source strengths and the circulation Γ are computed in the manner of panel methods by imposing a set of boundary conditions of specified normal velocity V_n at each panel control point, plus the Kutta condition at the trailing edge (Figure 4d). The solution is reached when f becomes small or after a finite number of iterations.

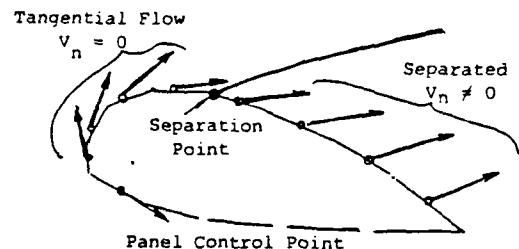


Figure 4d. 2-D Airfoil panel method analysis

e) The normal velocities computed for each span section are then used to modify the boundary conditions in the 3-D potential flow program used. The aerodynamic influence coefficient matrix [AIC] is unchanged. The vector σ is obtained by solving the equation

$$[AIC] [\sigma] = [b]$$

where σ is the unknown singularity vector (source and doublet strengths) and b is the vector containing the desired normal velocity components at all control points. The normal velocity vector V_{ni} at panel i control point is

$$V_{ni} = (\bar{V}_\infty + \bar{V}_Q) \cdot n$$

$V_{ni} = 0$ for attached flow and $\neq 0$ for separated flow. The specific values used are those obtained from steps d.

f) The modified boundary condition run results in a re-computed spanwise lift distribution which accounts for separation. The process may be repeated starting from step b, except that the solid line in Figure 4b could now be used instead of the dashed line, since "better" values of section lift are available.

Results and Discussion

First Phase of Development

The initial development of the present work was based on experimental results published in reference 5. There, a full scale wind tunnel test of a general aviation aircraft (complete configuration) was conducted. Several leading edge configurations were added and tested also. These results comprised pressure distributions at various span stations and lift coefficient curves up to $\alpha=40^\circ$. These were used to test the validity of the present method in very general terms.

A panel model for the wing alone was used in the computations, the fuselage was omitted for the sake of expediency. Some discrepancy was expected with the wind tunnel results for that reason. At that point in the development, only one iteration was performed, i.e., the pure potential flow analysis was done, followed by the computation of the normal velocities required to simulate the boundary layer thickness, based on the potential flow lift distribution $C_l(y)$, and finally a recomputation of the wing lift was done.

The computation was performed for the basic wing and one leading edge modification which has been tested. The curves in figure 5 are reproduced from reference 5. Also shown in figure 5 are the results of the computations shown with solid circles (basic wing) and squares (modified leading edge).

In these computations, 2-D airfoil data were required. Since there were no detailed 2-D data available for the tested airfoil section, the pressure data plots published in reference 5 were used. For the basic airfoil, the chordwise C_p distribution of the section closest to the plane of symmetry was used. For the cuffed airfoil, the section at the midpoint of the wing outboard panel with the leading edge cuff was used. These were considered close approximations of airfoil data even though they were taken from a finite wing. From the C_p plots, available for a range of angles of attack, the location of the separation point and the pressure coefficient from there to the trailing edge were plotted as functions of α , and used for the estimation of the "separated" boundary conditions.

A look at the total configuration lift coefficient for three angles of attack of 21.6° , 27° and 31.9° (figure 5) indicates that up to 27° , the computational model agrees with the experiment, whereas at 31.9° it did not, but the deviation is nearly the same for the two planforms which were compared.

The results at $\alpha=31.9^\circ$ are valid in the sense of evaluating the incremental effect of small planform modifications, a capability which is useful in designing such changes, with the intent of alleviating the sharp drop in lift after stall.

In figure 6, the computed pattern of the start of separation for various angles of attack is shown. On the outer panel, the separation occurs further downstream when the leading edge cuff is included. These plots are consistent with the oil flow photographs of reference 3.

These preliminary results, despite all the short-comings in the data used, were encouraging enough to pursue this work further.

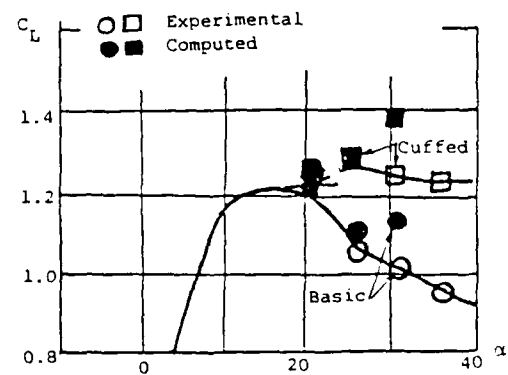


Figure 5. Comparison of computed and experimental lift coefficients of test wing.

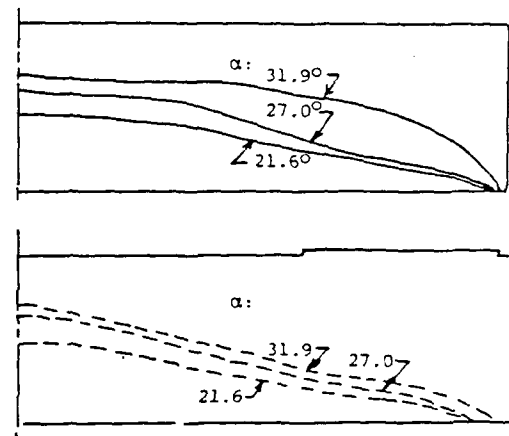


Figure 6. Computed stall pattern of basic and cuffed wings.

Second Phase of Development

New wind tunnel tests were started at Wichita State University using a simple rectangular wing with a NACA 24023 airfoil section and an aspect ratio of 13.3. In this test, pressure data were collected using a Strip-a-Tube belt.

These tests are still underway at the time of this writing, therefore only the analysis of the basic wing is performed. The objective is to test the convergence of the iterative scheme. The large aspect ratio and the fact that there is no fuselage helps determine the separation point and the 2-D lift coefficient more reliably. Plots of X_{sep} and C_{psep} for various angles of attack are depicted in figures 7 and 8.

The chordwise pressure was integrated to produce the experimental local lift coefficient. The C_l vs. α curves for various y locations are considerably different in magnitude, but the shape is similar. Airfoil data exists for this airfoil in reference 6 and was used because of the measurement error existing in the data due to the relative thickness of the Strip-a-Tube belt.

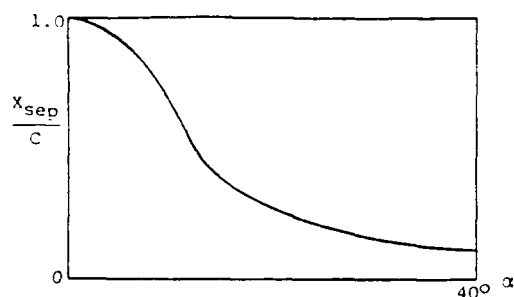


Figure 7. Location of the separation point.

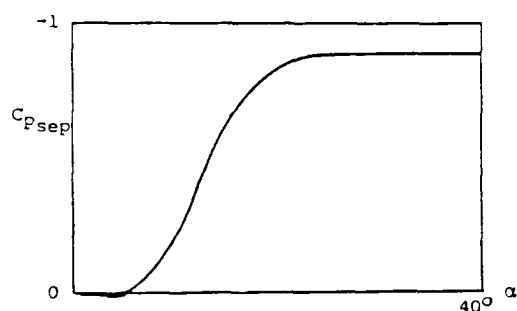


Figure 8. Upper surface pressure coefficient in the separated region.

The computational method was tested as follows:

- The panel method model was constructed for the wing using ten rows of chordwise panels.
- A pure potential flow ($V_n = 0$) run was performed for a wing angle of attack of 30° . The lift at the section nearest the plane of symmetry was considered the 2-D lift coefficient (value = 3.07) at $\alpha = 30^\circ$. At $\alpha = 0$, $C_L = 0.10$. A straight line interpolant was used to obtain the local angle of attack $\alpha(y)$ for determining x_{sep} and C_{psep} .
- The V_n vector was computed for each spanwise section and another potential flow run was made with the new boundary conditions. These V_n are based on the potential flow lift distribution and hence account for downwash.
- Some of the resulting section lift coefficient values cause a problem in finding the corresponding α since C_L is limited in range, except for the linear portion of the curve. For example, a C_L of 0.6 or less would imply a low local α (attached flow) even though it is known that the flow is highly separated at this point. On the other hand, a very large C_L is not realizable and no corresponding α exists. Iteration of the procedure thus necessitates a different approach for determining the $\alpha(y)$ for the next iteration.

The values of C_L fall outside the feasible range frequently because the α 's are over predicted or under predicted by the potential flow run, depending on the extent of the separation. Therefore, using the average C_L of the previous and current estimates is appropriate to help accelerate convergence. In addition, the largest value of C_L along the span is used along with the wing angle of attack to serve as one point on a 2-piece linear interpolant for α . The other two points required are the $\alpha = 0$ and its corresponding C_L , and C_{Lmax}

and its corresponding α . See figure 9. When the C_L values are within the feasible range, then the corresponding α 's are taken from the curve.

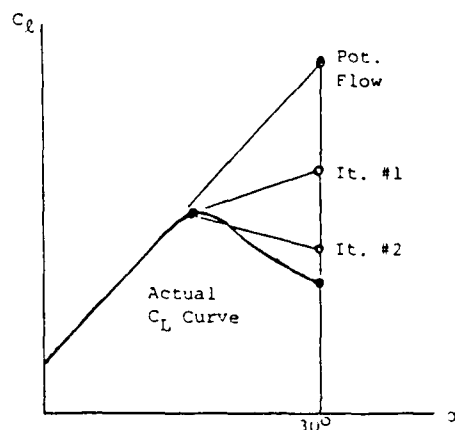


Figure 9. Intermediate lift curves for the computation.

e) By performing 4 iterations, the values of C_L appear to be converging toward the experimental data. The final results of the computation are compared with experiment in figure 10. The history of the convergence is shown in figure 11.

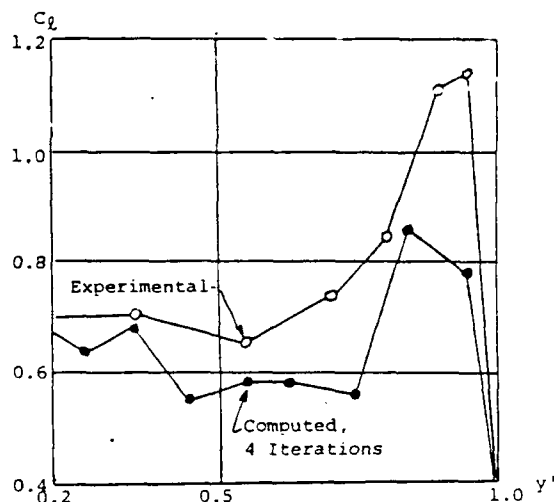


Figure 10. Computed and experimental lift distribution.

Conclusions

The method presented here is being developed as a part of a program dealing with stall/spin safety. It is intended to provide the preliminary designer with a quick way of determining effects of wing planform variations. Adding angular velocities to more clearly evaluate the aerodynamic moments of the wing can be done by further modifying the boundary conditions.

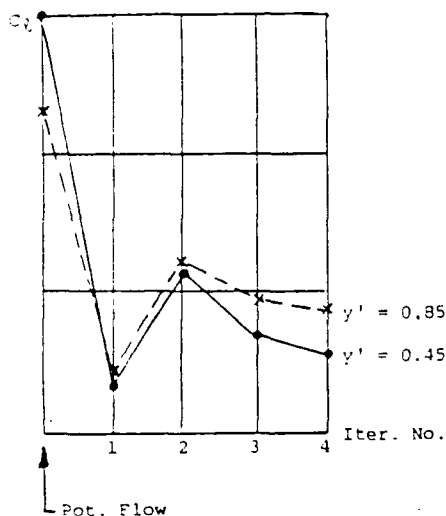


Figure 11. Convergence of the computed solution.

The method's known weaknesses are those due to some simplifications adopted for expediency. For example, in the estimation of the normal velocity components, a single lifting line approach was used, rather than a distributed vorticity. This led to some oscillations of pressure distributions near the trailing edge, and a large pressure peak at the leading edge. Further, the displacement of the vortex sheet away from the upper surface and a better application of the Kutta condition should improve the results. More runs to compare with existing data are required to refine and validate the method.

Its strengths are its simplicity, and the fact that it uses the reliable and familiar potential flow codes. The computing requirements are reasonable. So far, the comparisons with experimental data involved many approximations. It is desirable to conduct more testing with pressure taps for a variety of planforms. The results presented show much potential despite these weakness.

Acknowledgments

The authors wish to acknowledge the support of the Federal Aviation Administration Technical Center in Atlantic City, New Jersey, through contract #DTFA03-86-R-60039. The support and cooperation of the Flight Applications Branch staff of the NASA-Langley Research Center are also appreciated. Finally, they are grateful to Mr. George Ross, WSU graduate student, for making the early results of his wind tunnel tests available.

References

1. Wykes, J.H., et al, "An Analytical Study of the Dynamics of Spinning Aircraft," Wright Air Development Center, Tech. Rep. 58-381, Wright-Patterson Air Force Base, Ohio, Dec. 1958.
2. Ritter, J.R., "On Estimating Aircraft Nonlinear Rotary Derivatives from Static Wing Tunnel Data," Master's Thesis, The Wichita State University, (Institute for Aviation Research report, no. IAR 87-105) Wichita, KS, April 1987.

3. DiCarlo, D.J., et al, "Discontinuous Wing Leading Edge to Enhance Spin Resistance," J. Aircraft, Vol. 22, No. 4, pp. 283, April 1985.

4. Phutlek, P., "Experimental Investigation of Separated Flow Fields on a Wing with a Sharp Discontinuous Leading Edge to Improve Stall/Spin Resistance," Ph.D. Dissertation, The Wichita State University, (Institute for Aviation Research report, no. IAR 88-114) Wichita, KS, December 1987.

5. Newsom, W.A. Jr, et al, "Effects of Wing Leading Edge Modifications on a Full-Scale, Low-Wing General Aviation Airplane: Wind Tunnel Investigation of High-Angle-of-Attack Aerodynamic Characteristics," NASA Technical Paper 2011, June 1982.

6. Abbott, I.H. and VonDoenhoff, A.E., "Theory of Wing Sections," Dover Publications, New York, 1959.

APPENDIX C

WICHITA STATE UNIVERSITY INSTITUTE FOR AVIATION RESEARCH

Project Title: Stall/Spin Flight Simulation, Phase II: Spin Resistant Design and Spin Entry Detection

Principal Investigator(s): M.G. Nagati

Problem:

- Lack of a design methodology and tools for the design of spin resistant aircraft (non-linear, high angle of attack and angular rate aerodynamic analyses).
- Need for a "spin warning" device. Development requires the knowledge of parameters' behavior at onset of spin.
- Realistic evaluation of warning systems and spin-resistant designs requires flight simulator with special characteristics.

Objective:

- Develop aerodynamic analysis methods for wing, fuselage, empennage in the presence of high angular rates, separation and propeller wash.
- Identify parameters most dominant in spin entry and study behavior under a variety of conditions.

Accomplishments to date:

- Good simulation of aerodynamic forces and aircraft dynamic response has been established.
- Good prediction of stall pattern for isolated wing with and without leading edge extensions has been accomplished.
- Survey has been done of propeller wake prediction methods for twin engine aircraft.
- Graphics for flight simulation have been developed.

Brief work statement:

1. Complete simulator: install Learjet cockpit and add visual effect (computer graphics), checkout by test pilots.
2. Perform runs to identify spin entry parameters; develop requirements for "spin warning" device.
3. Select, acquire, and implement computational aerodynamic codes for arbitrary shapes with separated flows. Modify codes to allow for angular rates.
4. Continue development of modified panel method to obtain effects of leading edge shape on wing stall, and extension of technique to more arbitrary platforms.
5. Study and incorporate effects of fuselage and wing wakes on aerodynamic forces during spin.
6. Incorporate propeller induced flow effects.
7. Publish results.

Estimated costs: \$140,000 per year.